https://doi.org/10.5194/egusphere-2025-1358
Preprint. Discussion started: 7 May 2025


# Similarities between sea ice area variations and satellite-derived terrestrial biosphere and cryosphere parameters across the Arctic

Annett Bartsch[1], Rodrigue Tanguy[1], Helena Bergstedt[1], Clemens von Baeckmann[1], Hans Tømmervik[2], Marc Macias-Fauria[3], Juha Lemmentiynen[4], Kimmo Rautiainen[4], Chiara Gruber[1], and Bruce C. Forbes[5]

[1]b.geos, Industriestrasse 1, 2100 Korneuburg, Austria
[2]Norwegian Institute for Nature Research, Fram - High North Research Centre for Climate and the Environment, NO-9296 Tromsø, Norway
[3]Cambridge University, Cambridge, UK
[4]Finish Meteorological Institute, Helsinki, Finland
[5]University of Lapland, Rovaniemi, Finland

**Correspondence:** Annett Bartsch (annett.bartsch@bgeos.com)

**Abstract.** Satellite time series availability for the Arctic Ocean and adjacent land areas allows for cross-comparisons for cryosphere vs. vegetation parameters. Previous studies focused on correlation analyses between vegetation indices (derivatives of the normalized difference vegetation index (NDVI)) of tundra regions and sea ice extent for selected months. We have refined these analyses through consideration of distinct sea ice basins and all months, extension to south of the treeline, and included cryosphere essential climate variables such as snow water equivalent (SWE; March as proxy for annual maximum) and mean annual ground temperature (MAGT) in permafrost areas. The focus was on 2000-2019 considering data availability. As a first step, we derived trends. Changes across all the different parameters could be specifically determined for Eastern Siberia. Linkages between de-trended sea ice area (SIA) and NDVI across tundra regions was confirmed, where lower sea ice extent correlates with higher NDVI. The regional extension beyond the treeline revealed linkages for Northern European Russia and partially correlations of sea ice variations with land parameters over northern Scandinavia. Differences compared to previous studies ending in 2008 were found for the Kara Sea region and adjacent land area, indicating recent changes. In case of ground temperatures, high significant correlations were found for more distant sea ice basins than for NDVI, where the adjacent sea ice basins were more relevant. Negative and positive significant correlations can be found for March SWE depending on SIA month and region. Also, other months than September (sea ice extent minimum) were found to have high correlations vs. land-based variables, with distinct differences across sea ice basins. The fraction of data points with significant correlations north of 60°N is higher for SWE and MAGT than for the NDVI derivatives. Fractions for SWE are higher for Eurasia than Northern America. Autumn (incl. October and November) and mid-winter (incl. February, March) were most relevant for both investigated cryosphere-related parameters permafrost temperature and March snow water equivalent. Although similarities could be found between TI-NDVI and MaxNDVI, a higher proportion of significant correlations was observed for TI-NDVI. The datasets provide a baseline for future studies on common drivers of essential climate parameters and causative effects across the Arctic.

https://doi.org/10.5194/egusphere-2025-1358
Preprint. Discussion started: 7 May 2025


## 1 Introduction

Climate change across the Arctic affects specifically the cryosphere, including sea ice, ice caps and glaciers, snow and permafrost (IPCC, 2019). Feedback mechanisms and associated tipping systems of the global climate have been identified (Lenton et al., 2008; Armstrong McKay et al., 2022) and the potential of remote sensing for their monitoring discussed (Lenton et al., 2024). Recent sea ice extent and ice sheet mass balance decline can be well observed through the use of satellites (Spreen et al., 2008; Druckenmiller et al., 2021). Permafrost monitoring from space is limited but can be achieved through the use of land surface temperature in permafrost models (Westermann et al., 2017). Similarities in trends and variations have so far been identified between permafrost and ice sheets (Sasgen et al., 2024) and between permafrost and sea ice extent (Bartsch et al., 2023b, 2024). Sea ice variations have been also linked to vegetation patterns across the Arctic (e.g. Bhatt et al. (2010); Buchwal et al. (2020)). Variations of the cryosphere and biosphere on land are crucial for terrestrial ecosystems, including biodiversity (e.g. Rixen et al. (2022), MORE)).

Spatially and temporally consistent information going back in time is needed in order to reliably identify trends and patterns. Satellite records are limited to the last 40-50 years. Many records are much shorter, starting around 2000 CE or later. Data gaps and variable sampling intervals are additional challenges. Many Arctic climate change studies therefore rely on the use of re-analyzed data (e.g. Rantanen et al. (2022); Park et al. (2013)). Trends and linkages in related parameters observable from satellites have been nevertheless studied but are described usually for single parameters/pairs, or restricted to the current tundra and with varying analyses periods. Valuable information for understanding climate change patterns across the Arctic could be derived from satellite data despite its shortcomings but capabilities have not been fully exploited to date.

### 1.1 Trends based on satellite records

Trend analyses for the terrestrial Arctic based on multiple satellite derived parameters have been so far described by Comiso and Hall (2014) and AMAP (2017) (Table A1). Comiso and Hall (2014) focused on cryosphere-related parameters and applied a consistent time frame for the comparison. AMAP (2017) was based on a literature review and time frames thus therefore varied from parameter to parameter. Vegetation parameters were also not included in this case. The only common parameter discussed in the two studies was snow extent (Table A1). An update of trends has been published by AMAP (2021) considering also sea ice extent, but changing to a fusion of different sources in the case of snow parameters (modelling and satellite). Both studies included records starting in the early 1980s, but extend to differing years between 2010 and 2015. The southern limit of the analysis varied by up to 4° latitude.

A range of studies focused on Arctic trend analyses of single parameters (Table 1 and 2). Records from AVHRR (Advanced Very High Resolution Radiometer; shortwave and thermal infrared) and SSMR/SSMI (Special Sensor Microwave Imager; passive microwave) are crucial for analyses of changes back into the 1980s. Such comparably long records provide information related to the cryosphere (snow, albedo, sea ice, land surface temperature, freeze/thaw state) and vegetation (through the nor-

https://doi.org/10.5194/egusphere-2025-1358
Preprint. Discussion started: 7 May 2025


malized difference vegetation index - NDVI) records. Capabilities improved 1999 onward, starting with the MODIS (Moderate Resolution Imaging Spectroradiometer; shortwave and thermal infrared) sensor. Land surface temperature (LST) from MODIS was for example used for permafrost modelling (CryoGRID, Westermann et al. (2017); Obu et al. (2019)). Permafrost ground temperature estimated using various satellite records is available through the European Space Agency (ESA) Climate Change Initiative (CCI) covering the years 1997 to 2021. Specifically, mean annual ground temperature at 2m depth ($MAGT_{-2m}$) can be used as proxy for permafrost conditions, e.g. for the retrieval of permafrost extent (Obu et al., 2021b). Trends at 2m depth indicate that permafrost in Arctic coastal regions, specifically Siberia, is warming faster than others (Miner et al., 2022) (Table 1). Seasonal thaw depth (active layer thickness) is a further indicator for permafrost change. Western Siberia has been identified as a hotspot of change, with both increases in growing season length (Smith et al., 2004) and thaw depth (Brouillette, 2021). A statistically significant trend of increasing snow water equivalent (SWE) has also been reported over this region (Pulliainen et al., 2020), in contrast to decreasing trends over many other Eurasian regions as well as North America. SWE has also increased over Northern Fennoscandia according to satellite as well as in situ records (Bjerke et al., 2025). Surface temperature increase 1981-2012 was higher over the ocean than over land (Comiso and Hall, 2014). Different patterns over land can be observed between winter and summer over the last 40 years (Dupuis et al., 2024). Warming can be for example observed over mainland North America in winter and the Taymyr regions (Northern Eurasia) in summer. Both areas also show strong increases in MaxNDVI as derived from AVHRR (Frost, 2025).

Vegetation indices indicate changes across the entire Arctic tundra (Bhatt et al., 2017), with more pronounced patterns after 2000. Vegetation analyses rely specifically on NDVI retrievals from the GIMMS (Global Inventory Modeling and Mapping Studies) record which is based on AVHRR (different versions, 8x8 km) (Pinzon and Tucker, 2014) (Table 2). NDVI related trend analyses across the Arctic usually target the identification of greening or browning as a result of climate change (Bhatt et al. (2017), Frost (2025)). Greening is usually interpreted as increasing vegetation height, biomass, cover and abundance (Myers-Smith et al., 2020). Most studies therefore focused on specific NDVI statistics rather than phenology. The main target parameters are MaxNDVI and TI-NDVI. MaxNDVI is the maximum annual NDVI and TI-NDVI the sum of summer bi-weekly NDVI. Spatial patterns between MaxNDVI and TI-NDVI trends differ (Frost, 2025). MaxNDVI trend patterns captured by MODIS (500m) are more pronounced than the higher spatial resolution observations based on Landsat (30m, Frost (2025)). An alternative to TI-NDVI is growing season summed NDVI (GSSNDVI). It is based on daily NDVI values, which is of limited applicability due to frequent cloud cover but which is a good proxy for gross primary production across the Arctic (Park et al., 2016). Phenology indicators based on AVHRR NDVI indicate an increasing length in growing season in many parts of the Arctic (Park et al., 2016).

## 1.2 Linkages with sea ice variations

### 1.2.1 Vegetation

Previous regional NDVI studies indicated the importance of sea ice in basin specific analyses (e.g. Bhatt et al. (2010); Macias-Fauria et al. (2012, 2017); Table 3). Sea ice basin specific TI-NDVI (AVHRR) trend relationship analyses covering the entire

https://doi.org/10.5194/egusphere-2025-1358
Preprint. Discussion started: 7 May 2025


**Table 1.** Past studies on Arctic trends with focus on observables from satellite data (excluding ice sheets) - part I.

| Parameter | Source | Time period | Trend observation |
|---|---|---|---|
| Permafrost mean annual ground temperature (CryoGRID using MODIS LST and reanalyses) | Miner et al. (2022) | 1997-2018 | Ground temperatures at 2m depth have been increasing especially in coastal regions. Most affected regions are northern Yakutia and the northern part of the Yamal Peninsula with more than 1°C increase per decade. |
| Active layer thickness (CryoGRID using MODIS LST and reanalyses) | Brouillette (2021) | 2007-2016 average vs. 1997-2006 | ALT deepened on average by 2.5 cm across the Northern hemisphere. Some of the highest rates across the Arctic can be observed for Western Siberia. |
| Freeze/thaw (SSMR and SSMI) | Smith et al. (2004) | 1988-2001 | Earlier thaw in Eurasia, later freeze in North America. Increasing growing season length over Western Siberia/Yamal . |
| Snow water equivalent (SSMR and SSMI) | Pulliainen et al. (2020) | 1980-2018 | Notable variability in trends across the Arctic. Increasing SWE over Western Siberia, Russian far east and northern Scandinavia. Visible trends of decreasing SWE for North America and southern Fennoscandia. |
| Snow cover extent (incl. AVHRR) | Comiso and Hall (2014), AMAP (2017) | 1967-2012 | Spring: 2.7% reduction per decade for the entire northern hemisphere. This value is similar for Eurasia, less (1.27%) in case of North America. |
| Snow melt off (SSMR and SSMI) | Pulliainen et al. (2020), Takala et al. (2009) | 1979-2014 | Earlier spring snow melt-off (day of snow clearance in boreal forest zone of the Northern hemisphere (-3.04 d/decade in Eurasia, -1.27 d/decade in North America) |
| Spring snow melt and albedo (AVHRR) | Anttila et al. (2018) | 1982-2015 | Albedo decrease before snowmelt mostly in Fennoscandia, earlier start of snowmelt in central Siberia (North; and partially earlier end of melt), melt season duration decreased slightly for Alaskan North Slope. |
| Sea ice extent (SSMR and SSMI) | Comiso and Hall (2014) | 1979-2012 | Decline of sea ice extent (-3.8% per decade) and concentration across the Arctic with highest magnitude to the North of Franz-Joseph-Land. |
| Sea ice extent (SSMR and SSMI) | Stroeve and Notz (2018) | 1979-2018 | On average -2.6% and -11.3% per decade in March and September respectively. |
| Albedo (AVHRR) | Comiso and Hall (2014) | 1982-2012 | Reduction over land by 0.5% per decade in April and 0.17% for May. But increasing Albedo for Western Siberia and partially the Kola peninsula. |
| Land and sea surface temperature (AVHRR) | Comiso and Hall (2014) | 1981-2012 | Increasing surface temperatures across the Arctic (>64°, 0.69°C per decade). Higher increase over the Arctic ocean and Greenland than over land. |
| Land surface temperature (AVHRR) | Dupuis et al. (2024) | 1981-2020 | Increasing surface temperatures in the proximity of the Taymyr peninsula and Canadian High Arctic, decreasing close to parts of the Beaufort Sea in summer. Increase over North America and Scandinavia in winter. |
| Cloud cover fraction (AVHRR) | Comiso and Hall (2014) | 1981-2012 | Decrease by 2 % per decade for the entire Arctic. Higher values over Greenland, less over other land areas, Eurasia 1.22% decrease. |

https://doi.org/10.5194/egusphere-2025-1358
Preprint. Discussion started: 7 May 2025


**Table 2.** Past studies on trends with focus on observables from satellite data - Part II: Arctic tundra MaxNDVI and TI-NDVI.

| Sensor | MaxNDVI | TI-NDVI | Source | Time period | Trend observation |
|---|---|---|---|---|---|
| AVHRR (GIMMS) | X | X | Bhatt et al. (2017), AMAP (2017) | 1982-2015 | Greening Alaskan North Slope and eastern Taymyr, browning West Siberia, North Yamal to West Taymyr, SW Alaska and Canadian high Arctic; TI-NDVI declining trends since 2000 together with Summer Warmth Index. In general, trends for the whole time period come from changes after 2000. Linkages with sea ice weekly mean. |
| | X | | Liu et al. (2024) | 2000-2015 | MaxNDVI increase on parts of the Alaskan North Slope and Western Taymyr. |
| | X | X | Frost (2025) | 1982–2023 | MaxNDVI increase across mainland North America and Eastern Taymyr. Decline across European Russian Arctic. Similar patterns for TI-NDVI. |
| MODIS | X | | Liu et al. (2024) | 2000-2015 | MaxNDVI increase on parts of the Alaskan North Slope and Western Taymyr similar to AVHRR. |
| | X | X | Frost (2025) | 2000–2023 | MaxNDVI increase on parts of the Alaskan North Slope and Western Taymyr. Different patterns for TI-NDVI. |
| Landsat | X | | Berner et al. (2020) | 1985-2016 2000-2016 | Tundra greenness increased (greening) at ∼37.3% of sampling sites and decreased (browning) at ∼4.7% of sampling sites. Differences between 2000-2016 and full period analyses. |
| | X | | Frost (2025) | 1984-2023 2000–2023 | MaxNDVI increase on parts of the Alaskan North Slope, Western Taymyr and eastern Canada. Pronounced decline for eastern Taymyr and Northern Yakutia. |
| | X | | Liu et al. (2024) | 2000-2020 | Increase specifically across Canada |

Arctic has been initially carried out for a 50km – 100km buffer (for land area north of tree line, as defined through the CAVM, Walker et al. (2002), Raynolds et al. (2019)) covering the years 1982 to 2008 (Bhatt et al., 2010) (Table 3). The timing of the 50% mean sea ice concentration in spring was used for these analyses. Significant correlations were found for Eastern Siberia (Bering, Chukchi, Laptev, East Kara) and the Canadian Archipelago. Further analyses were made for de-trended MaxNDVI (Bhatt et al., 2013) and a longer time period (to 2019; Bhatt et al. (2021)) separating Eurasia and Northern America. Initially, a 100km ocean zone with a focus on open water data was compared to tundra over adjacent land area by sea ice basin including data until 2008 (20 basins, Bhatt et al. (2013)). This was extended to 2019 including also summer average open water extent, but with separation between North America and Eurasia only (within the tundra CAVM boundary, Bhatt et al. (2021)). Statistically significant correlations were only found for North America, compared to TI-NDVI which was relevant for both regions. This applied to the time period 1982-2019 as well as to the original 1982-2008 records. Li et al. (2023) demonstrate issues with orbital drift in GIMMS/AVHRR records. Trends derived from GIMMS were also shown to differ from MODIS (Frost, 2025).

https://doi.org/10.5194/egusphere-2025-1358
Preprint. Discussion started: 7 May 2025


Dutrieux et al. (2012) focused on central and eastern Siberia using for the first time MODIS data (2000-2011). Correlations of TI-NDVI with sea ice cover decline with the distance from coast. Highest correlations were found for mid-June sea ice concentrations. Yu et al. (2021) investigated monthly sea ice data and identified a link between summer months NDVI with summer sea ice extent without time lag for central to eastern Siberia and Alaska (within the CAVM extent). Late spring (May – early June) sea ice was also compared to NDVI for Western Siberia in Macias-Fauria et al. (2012). Comparably high correlations were found for the European part for May.

Kerby and Post (2013) focused on Kangerlussuaq (West Greenland) and the relationship of sea ice (January to May) with the summer warmth index which was linked in previous studies to NDVI in other regions (Bhatt et al., 2021). Highest correlation was found for the Davis strait/Baffin Bay regional sea ice extent in June. An influence of adjacent sea ice variations on NDVI was also found for northernmost and eastern Svalbard (Macias-Fauria et al., 2017; Karlsen et al., 2024).

### 1.2.2 Permafrost

The lower the NH minimum sea ice extent, the higher the NH mean annual ground temperature in permafrost soils (Bartsch et al., 2023b). The relationship of permafrost (MAGT at 2m depth) and NH sea ice trends has been initially investigated for September conditions (minimum extent; meereisportal.de (Spreen et al. (2008), grant: REKLIM-2013-04)). The overall trend for the northern hemisphere MAGT at 2m depth (referring to the area of permafrost extent maximum within the observation period, 1997–2019) follows sea ice decline for September ($R^2$= 0.75). A change of on average one degree Celsius at 2 m depth coincides with September sea ice decline of about 2.5 million km$^2$. This analysis was extended covering all months and detrending was applied (Bartsch et al., 2024). The correlation of $MAGT_{-2m}$ with monthly NH sea ice extent was shown to be comparably high from August to October ($R^2 > 0.8$) in all cases, but regional differences (on land) have been identified across the Arctic. Correlation was highest for Northern Central Siberia. This differs from areas with highest trends for ground temperature as shown in Miner et al. (2022). The latter are located more eastwards. Sea ice basin specific analyses have not been reported to date.

### 1.2.3 Snow

The impact of sea ice conditions on snow parameters has been investigated on the basis of modelling, specifically for SWE. The used sea ice records were usually representing September as the month of minimum extent and analyses considered averages for the entire Arctic (Park et al., 2013). Low sea ice cover was found to be linked to anomalously high snow depth (as determined by the land surface model CHANGE) in northeast Siberia for 1979 to 2006 due to increase in precipitation (Park et al., 2013). In contrast, a decline in snow depth was found for North America.

Gastineau et al. (2023) found declining trends in snow mass across eight different models for 1979-2014, with high deviations in absolute values among the models. The sea ice correlation analyses were thus limited to the parameter snow extent. The focus was on the months from November to March for both snow extent and sea ice. No robust influence of sea ice con-

https://doi.org/10.5194/egusphere-2025-1358
Preprint. Discussion started: 7 May 2025


**Table 3.** Past studies on NDVI and sea ice correlation analyses.

| Source | Parameters | Sensors for NDVI/Sea ice | Time period | Analysed Sea ice basin | Analysed land area | Comments on method | Result |
|---|---|---|---|---|---|---|---|
| Bhatt et al. (2010) | TI-NDVI<br>Timing of mean (50%)<br>sea ice concentration | AVHRR/ SSM/I<br>Comiso and Nishio (2008) | 1982-2008 | All Arctic, North America,<br>Northern Eurasia and<br>basin specific | 50-100km buffer<br>near specific basin | | Significant trend relationship for<br>Eastern Siberia<br>and Canadian Archipelago |
| Bhatt et al. (2013) | TI-NDVI<br>MaxNDVI<br>Sum of weekly May through<br>August open-water percentage | AVHRR/SSM/I<br><br>Comiso and Nishio (2008) | 1982-2008 | All Arctic, North America,<br>Northern Eurasia and<br>basin specific | CAVM extent,<br><300m | detrended | MaxNDVI significant trends<br>only for Northern America |
| Bhatt et al. (2021) | TI-NDVI<br>MaxNDVI<br>Timing of mean (50%)<br>sea ice concentration<br>Summer OW average of<br>weekly May through<br>August OW percentage | GIMMS NDVI3g<br>V1.2 product/ SSM/I<br><br>Comiso and Nishio (2008) | 1982-2019 | All Arctic, North America,<br>Northern Eurasia | CAVM extent,<br><300m | detrended | MaxNDVI significant trends<br>only for Northern America |
| Dutrieux et al. (2012) | TI-NDVI<br>Timing of mean (50%)<br>concentration<br>Sea ice extent | MODIS/<br><br>NSIDC-0002/81 | 2000-2011 | Eight selected sea areas<br>defined by 150 km radius | extent in central and<br>eastern Siberia | Detrended, for<br>distance analyses<br>50-300km<br>transects starting at<br>the ocean within CAVM | Correlations decline by<br>distance from coastline |
| Yu et al. (2021) | Monthly NDVI,<br>Monthly sea ice concentration<br>(all year), area and extent | 15–day GIMM3g/<br>HadISST.2.1.0.0 | 1982-2015 | All Arctic | CAVM extent | if SIE exceeds 15%.<br>All data brought<br>into 100km grid<br>Mann-Kendall trend test,<br>Pearson correlation,<br>time lag analyses<br>(land grid cell specific) | Link between summer month<br>NDVI and with summer sea ice<br>extent without time lag for<br>central to eastern Siberia and Alaska |
| Macias-Fauria et al. (2012) | Bi-weekly to Monthly NDVI,<br>monthly sea ice area<br>(May to August) | GIMMS AVHRR<br>/NSIDC-0079 | 1992-2005 | Baranets & Kara sea | Western Siberia | Pearson correlation<br>accounting for<br>autocorrelation | Comparably high correlations were<br>found for the European part for May. |
| Macias-Fauria et al. (2017) | 8 day mean NDVI, 8 day<br>mean Sea ice concentration | AVHRR + MODIS<br>for gap filling,<br>Norwegian Sea Ice<br>Service (SAR and<br>passive microwave<br>combined) | 2000-2014 | Area around Svalbard,<br>east and west half | Svalbard, east and<br>west half | Singular value<br>decomposition | influence of sea ice on NDVI was<br>found for northernmost Svalbard,<br>but not other parts |
| Karlsen et al. (2024) | 8 day mean NDVI, 8 day<br>Mean Sea ice cover (May<br>to September) | integrated MODIS-NDVI<br>(onset to peak growing<br>season), Norwegian Sea Ice<br>Service (SAR and<br>passive microwave<br>combined) | 2000-2022 | Area east of Svalbard | Svalbard | | general influence of<br>sea ice on NDVI was<br>found for Svalbard |
| This study | MaxNDVI, TI-NDVI,<br>monthly sea ice area<br>(all year) | MODIS, OSISAF | 2000-2019 | All Arctic and several basins | >60°N and CAVM | Detrended,<br>Pearson correlation,<br>land grid cell specific | |

centration variability on snow cover extent was found, which was attributed to the lack of ocean-sea ice coupling in the models (Gastineau et al., 2023).

135

A linkage between lake ice growth across Alaska and September sea ice concentration in the adjacent ocean (Beaufort and Chukchi Seas) was found for records from 1991-2008 (Alexeev et al., 2016). It was suggested that sea ice conditions impact snowfall on land based on an investigation of SWE obtained from regional climate model simulations driven by reanalysis data. Low sea ice cover was found to lead to higher precipitation/SWE and thinner lake ice due to the insulation effect of snow.

140 On a pan-Arctic scale, neither a splitting into basins nor the consideration of other months than September sea ice extent has

https://doi.org/10.5194/egusphere-2025-1358
Preprint. Discussion started: 7 May 2025


been analyzed so far based on satellite derived snow records.

#### 1.2.4 Objectives

Linkages of observables across the North Pole have been recently documented for selected cryosphere parameters. In this study, we present a pan-Arctic analysis and discussion of similarities between sea ice variation and observed terrestrial biosphere and cryosphere parameters. This is needed to advance our understanding of processes conditioning climate change impacts across the Arctic, but is lacking to date. Previous circumpolar analyses of NDVI focused on sea ice comparisons within the adjacent basins only. Also, analyses were confined to tundra regions. They were defined through the boundaries of the CAVM, which excludes among other regions, Northern Scandinavia and Northwestern Russia. While there are limitations for records based on satellite data, spatially and temporally consistent observations are available for some parameters 2000 onward. In order to address these gaps, we analysed time series of both TI-NDVI and MaxNDVI, permafrost ground temperature and snow water equivalent, considering multiple sea basins for identification of potential regional linkages (confined to area north of 60°N).

## 2 Data and methods

### 2.1 Datasets and analyses extent

Sea ice area (SIA) records were obtained from the EUMETSAT OSI SAF (Ocean and Sea Ice Satellite Application Facility) Sea ice index (version 2.1 (2020), OSI-420, OSI SAF and EUMETSAT SAF On Ocean And Sea Ice (2020)). SIA represents the sum of the total cover area of a given pixel multiplied by the ice concentration in that pixel. The extents of the sea ice basins were used as defined through the data provider (OSISAF). This includes eight basins covering most of the Arctic except the Canadian Archipelago (retrieval impeded due to limited extent of water surface between islands) (Figure 1).

Vegetation, permafrost and snow records were considered for the sea ice correlation analyses (Table 4). The analyses period has been harmonized across the available datasets. The overlap period has been defined as 2000-2018/19, which allows the usage of MODIS for vegetation records as well as permafrost time series. The analyses of vegetation parameters included MaxNDVI and TI-NDVI following previous studies (Table 1 and 2). MODIS NDVI data were extracted from Tømmervik (2025). Records are available at 250 m nominal resolution.

Ground temperature is available from the ESA CCI Permafrost project (v2 Obu et al. (2021a)). It is derived from a thermal model driven and constrained by satellite data (MODIS LST). Average annual ground temperatures are provided for specific depths (surface, 1m, 2m, 5m , 10m) and at 1km gridding. This dataset covers the Northern Hemisphere (north of 30°) for the period 2003-2021 based on MODIS Land Surface temperature merged with downscaled ERA5 reanalysis near-surface air temperature data in case of cloud cover. Whereas active layer thickness is also available, this variable was not considered since

https://doi.org/10.5194/egusphere-2025-1358
Preprint. Discussion started: 7 May 2025


uncertainties are higher than for ground temperature (Heim et al., 2021).

SWE is available from the ESA GlobSnow v3.0 climate data record (Takala et al., 2009; Luojus et al., 2021; Pulliainen et al., 2020). The data are provided in a fixed equal-area grid (EASE grid) of 625 km$^2$, nominally at 25 km by 25 km spatial resolution. Islands, areas with notable topography such as mountain ranges as well as the comparably ice-free but narrow margin of Greenland were masked. The dataset is derived from passive microwave observations (SSMI). Average SWE in March was selected for this study and interpreted to represent maximum SWE conditions.

To facilitate the discussion, number of frozen days (obtained from the MEAsUREs dataset and based on passive microwave, Kim et al. (2017, 2021)), aggregated Landsat MaxNDVI trends (Mekonnen et al., 2021) and MaxNDVI available from the GIMMS/AVHRR dataset (Pinzon and Tucker, 2014; Vermote and NOAA CDR Program, 2019) were used. The general analysis extent for the land parameters was set to be north of 60°N. Subsets for tundra only, based on the CAVM, were created for comparability with previous studies (see Table 3). The east and west boundaries of these subsets are extensions of the eight sea ice basins towards south.

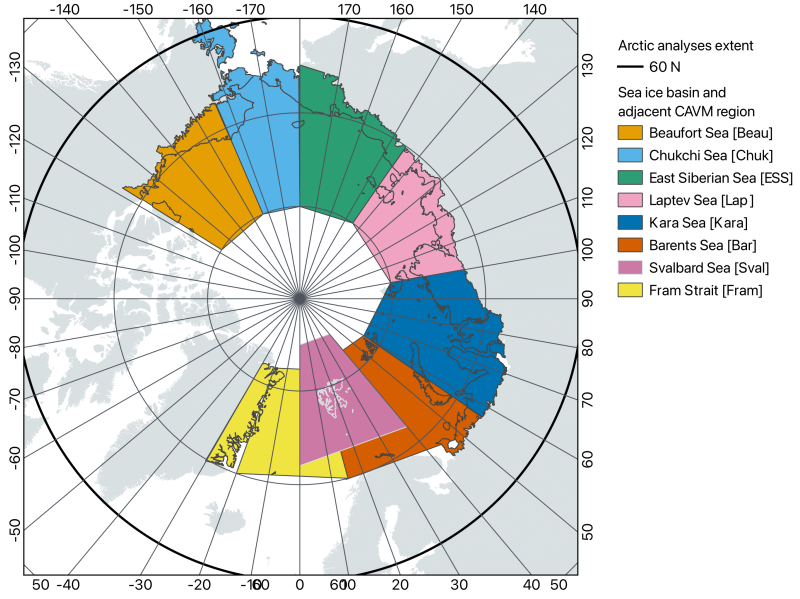


**Figure 1.** Ocean basins considered for sea ice area correlation analyses as defined by "OSI SAF Sea Ice Index v2.1" (OSI SAF and EUMETSAT SAF On Ocean And Sea Ice, 2020) and adjacent land area confined by the southern CAVM (Walker et al., 2002)) boundary (treeline), and full analyses extent north of 60°N.

https://doi.org/10.5194/egusphere-2025-1358
Preprint. Discussion started: 7 May 2025


**Table 4.** Datasets considered for correlation analyses covering the entire Arctic

| Parameter | Unit | Spatial detail | Temporal detail | Source | Reference | Used time period |
|---|---|---|---|---|---|---|
| MaxNDVI<br>TI-NDVI | - | 250m | annually | MODIS | Tømmervik (2025) | 2000-2019 |
| Mean annual ground temperature at 2m | °C | 1km | annually | MODIS LST/ Reanalyses (ESA CCI+ Permafrost v2) | Obu et al. (2021a) | 2000-2019 |
| Snow water equivalent | mm | 25km | monthly | SSMI (ESA GlobSnow v3) | Pulliainen et al. (2020)<br>Luojus et al. (2021) | 2000-2018 |
| Sea ice area | $km^2$ | basin scale | monthly | OSISAF | OSI SAF 2020 | 2000-2019 |

## 2.2 Trend and correlation analyses

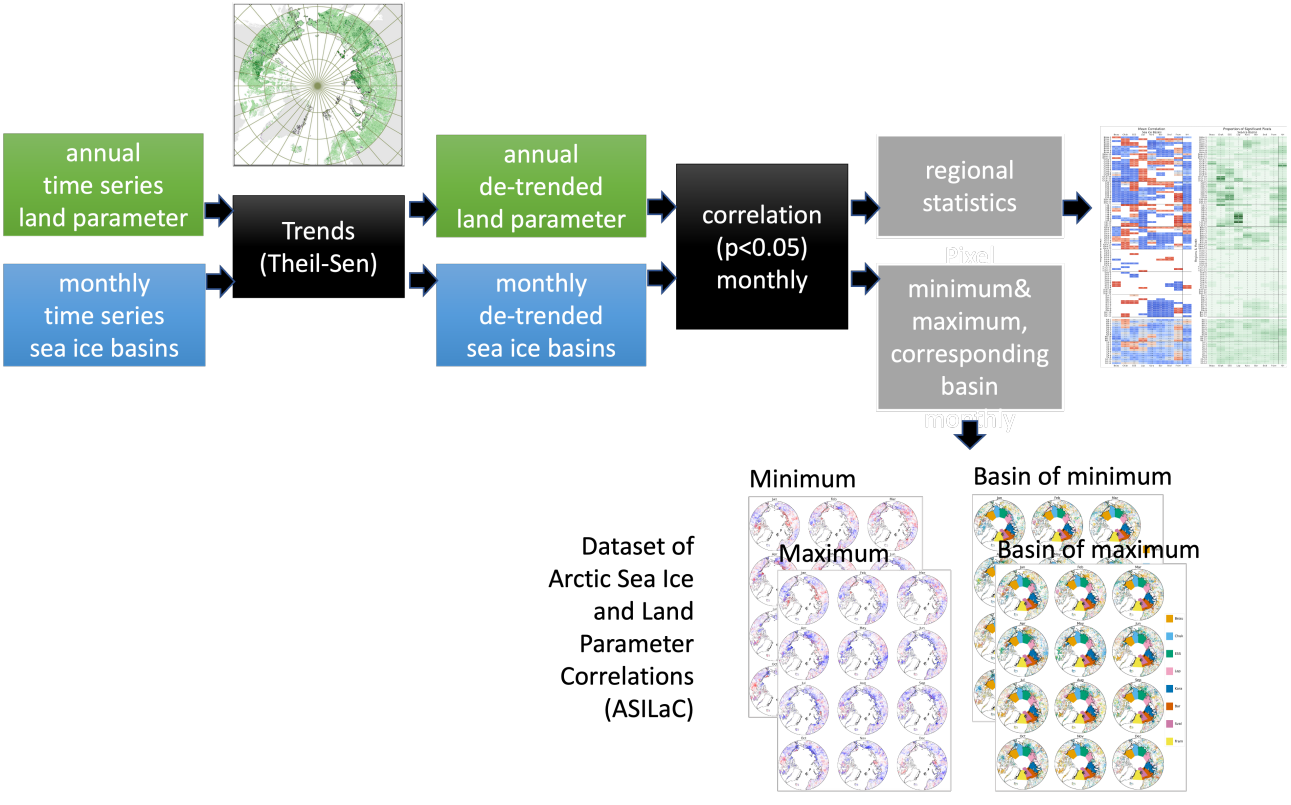


**Figure 2.** Workflow overview. Figure examples represent TI-NDVI. Trends and regional statistics are presented in the results sections, maps of all data are included in the dataset of Arctic Sea Ice and Land Parameter Correlations (ASILaC) and in the appendix.

https://doi.org/10.5194/egusphere-2025-1358
Preprint. Discussion started: 7 May 2025


The main workflow comprised trend retrieval, de-trending, correlation analyses and post-processing for the creation of the dataset of Arctic Sea Ice and Land Parameter Correlations (ASILaC) (Figure 2).

Dedicated pre-processing was only required for the extraction of frozen days, which served as auxillary dataset. We used data from the MEAsUREs dataset that includes both AM and PM orbits. A pixel was considered frozen only if retrievals from both overpasses (AM and PM) =estimated a frozen state. Trend analysis was applied to the cumulative number of frozen days from 1-Mar to 31-Jul.

First, trends were derived for all land parameters as listed in Table 4 and for >60°N. Consistent masking (land/sea, lakes, glaciers) was applied to all datasets. Trends were derived using Theil-Sen analyses. In the case of MaxNDVI, trends were also determined based on records from AVHRR/GIMMS.

In a second step, de-trending was applied. The Pearson correlations of sea ice area with the land parameters were determined for the entire NH and sub-basins. Monthly SIA was compared to mean annual ground temperature ($MAGT_{-2m}$), TI-NDVI, MaxNDVI and SWE (March, representing annual maximum). In the case of SWE, January to March SIA represents the same year and April to December the previous year. In all other cases, January to December of the same year were used. For all further analyses, only significant correlations were considered ($p < 0.05$).

Results of the correlation analysis include gridded datasets of pixel-wise correlations with each sea ice extent area. Masking was applied with respect to significant correlation on a per-pixel basis. The pixel-specific minimum and maximum correlation values - including corresponding month and sea ice basin - were determined and included into ASILaC. Results were summarized for the CAVM sub-regions, North America and Northern Eurasia. This included average correlations and the proportion of pixels with significant correlations for each region.

## 3 Results

### 3.1 Trends

SWE has been both increasing and decreasing across the Arctic during the analysis period 2000-2019 (Figure 3). On average, it has, however, increased north of 60°N (Table A2). Permafrost ground temperature and NDVI indices have also mostly increased. Large changes were observed for NE Siberia across these parameters, except TI-NDVI. Parts of Western Siberia and Northeast Siberia which experienced increasing snow amount showed also higher positive trends of MaxNDVI. Smaller patches of decreasing as well as increasing NDVI-based variables were found south of the treeline, likely reflecting vegetation response to e.g. fires.

https://doi.org/10.5194/egusphere-2025-1358
Preprint. Discussion started: 7 May 2025


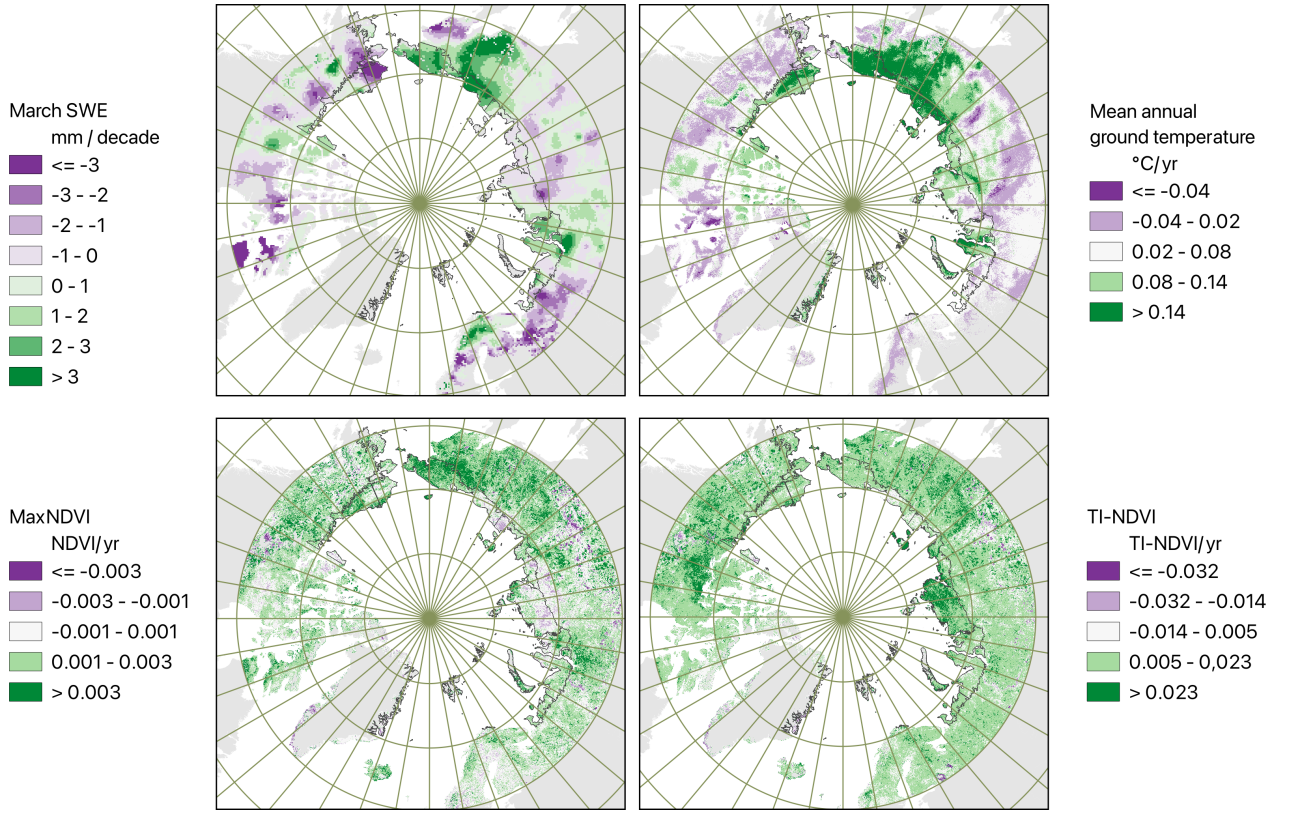


**Figure 3.** Trends for Snow Water Equivalent (SWE), Mean Annual ground Temperature, MaxNDVI and TI-NDVI (2000 - 2018, data sources see Table 4). Black outlines represent CAVM extent (source: Walker et al. (2002)).

### 3.2 Correlations

The proportion of area with significant correlation ranged from zero to 95% (Figures 4, 5, 6, 7). Values were higher for SWE and MAGT than for vegetation parameters and lowest for MaxNDVI. This applied to the tundra (CAVM) regions as well as larger area analyses (Figure 8). While in most cases values were below 10% within the CAVM regions, in some cases much larger values were obtained. Svalbard non-glaciated area reached proportions of more than 90% significant correlations in the case of MAGT for January SIA condition in the Svalbard sea and January and February SIA conditions in the Barents Sea. 64% were obtained for March SWE in case of the Beaufort Sea region linked to Fram Strait SIA in October. Considering the full Northern Hemisphere SIA, February was most important for SWE in the Laptev Sea coastal region (61%). Proportions for TI-NDVI exceeded 50% for the linkage of the Barents Sea and Laptev sea with their adjacent area in August. The lowest values were observed for MaxNDVI, with at maximum 30% in the case of the Barents CAVM area and January SIA in the Kara Sea.

https://doi.org/10.5194/egusphere-2025-1358
Preprint. Discussion started: 7 May 2025


North of 60°N proportions were higher for Northern America than for Eurasia in case of TI-NDVI, MaxNDVI and MAGT. This pattern is reversed for SWE. This largely also applied when confining the analyses to tundra regions, except for MAGT. The significant fractions were comparably low for the region adjacent to the Beaufort Sea ice basin (what includes the Alaska North Slope).

Proportions for MAGT were the highest among the investigated parameters, exceeding 90% for Svalbard (for Svalbard Sea sea ice in January and Barents Sea ice are in January and February) and 80% for the Laptev Sea coastal region when considering the entire NH sea ice record (August). Results for the Fram strait and Svalbard adjacent land areas were unavailable for SWE due to the masking of ice sheets and coarse spatial resolution for the used records.

### 3.2.1 Sea ice and permafrost

The relationship between sea ice extent and MAGT differed among the investigated regions, months, and Arctic ocean basins. In general, the correlations were negative; that is, as sea ice area declines, ground temperatures increase (Figures 4,A3). Northern central Siberia (Yamal to Lena Delta - Kara to Laptev sea region) and the Canadian Archipelago had the strongest relationship with sea ice in July to October. Not only summer but also most cold season months SIA were relevant for Eastern Siberia (October to May, except December) and specifically for Svalbard and NE Greenland (December to May).

The fractions of land areas with significant correlations were in many cases lowest for December and highest for May to October. MAGT variations for most of Western Siberia and North West Russia were linked to sea ice patterns of the relatively close Fram Strait in August to September and of the Kara Sea in October and November (Figure A4). Average correlations for tundra were around -0.5 (Figure 4). The Chukchi Sea ice showed strong statistiscal links to changes in adjacent land areas and Eastern Siberia in several months, specifically in transition periods. Negative correlations occur in early winter, with >50% of pixels with significant values. The Chukchi Sea CAVM region MAGT is relatively highly negatively correlated with cold season SIA of the Chukchi Sea in addition to the East Siberian SIA in Autumn.

Significant correlations with more distant basins were found in many cases. Chukchi Sea and Beaufort sea ice variations were inversely correlated MAGT (< -0.5 on average, 63% significant) in parts of Western Siberia (Kara) for October. Central Siberian MAGT correlated with the East Siberian Sea ice in August to October and the Beaufort SIA for January to June (Figure A4). Variations were also similar for the Canadian Archipelago MAGT and the Kara Sea SIA from March to June in addition to the Beaufort SIA in September and October. Northern Fennoscandia showed partial similarities with Barents and Kara SIA from January to September. Some sites in its western part correlated with Eastern Siberian Sea, Chukchi Sea and Beaufort Sea ice variations in October to December. The MAGT of the Laptev Sea tundra regions co-varies with sea ice along its coast from May to October. In addition, Summer to Autumn SIA of the Beaufort Sea is significantly negatively correlated across the Laptev Sea tundra. The entire northern hemisphere SIA from spring to autumn negatively correlated most with the Laptev Sea CAVM region, with up to 80% significant pixels, which are the highest values for all analysed parameters.

https://doi.org/10.5194/egusphere-2025-1358
Preprint. Discussion started: 7 May 2025


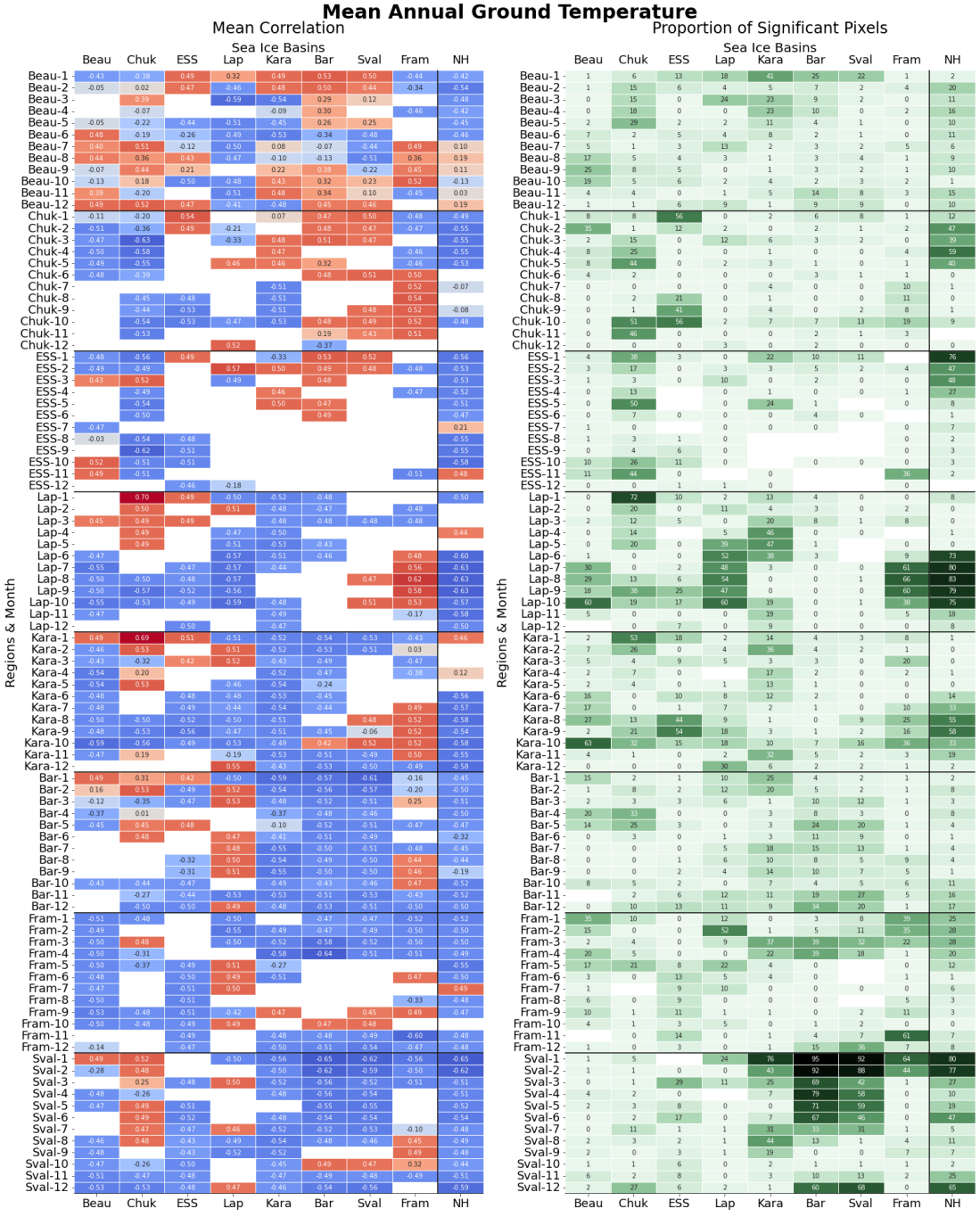


**Figure 4.** Significant correlations (95%) and proportion of significant pixels for sea ice (by basin) versus mean annual ground temperature within CAVM regions (see Figure 1 for abbreviations and Table 4 for data sources).

https://doi.org/10.5194/egusphere-2025-1358
Preprint. Discussion started: 7 May 2025


Higher values are only reached in case of the linkage between the Svalbard and Barents SIA with the Svalbard unglaciated area.

Regionally, positive correlations were also observed. Chukchi Sea January and February sea ice area was for example positively correlated with MAGT along the Kara Sea tundra region (0.53 to 0.69; 26-53% proportion of significant values). Positive correlations were also found regarding the August and September Fram Strait sea ice extent. August to October SIA for the Beaufort to Laptev Sea regions were negatively correlated with MAGT of the Kara Sea region. Positive significant correlations can be found for Summer to Autumn SIA conditions in the Fram Strait across all CAVM regions except the East Siberian Sea.

### 3.2.2 Sea ice versus MaxNDVI & TI-NDVI

Both negative and positive correlations between MaxNDVI and SIA were found (Figures 5,A5). However, the highest significant fractions are negative, with more greening in cases of low sea ice extent. The same applies to TI-NDVI (Figures 6,A2, A8). Distinct high positive correlations were found for the Chukchi Sea ice area across several regions (Figures A9, A10). The results of the two indices show partially similar spatial patterns. Significant trends can be observed for Far Eastern Siberia in both cases. In April to May, central to eastern Siberian values increased, specifically related to sea ice variations in the Chukchi region for MaxNDVI and related to Beaufort SIA for TI-NDVI. This region has been also identified as relevant for TI-NDVI by Bhatt et al. (2010). July to December SIA variations of the Beaufort, Chukchi and East Siberian Seas showed similarities with MaxNDVI as well as TI-NDVI across the European Russian Arctic and Western Siberia. The highest proportion of significant pixels and strongest negative correlations with TI-NDVI was obtained for the summer Laptev and East Siberian Sea ice area and the adjacent land area (57% and 47% respectively). The Chukchi Sea tundra area TI-NDVI variations coincided with lower sea ice extent in the Chukchi Sea region. Higher proportions of significant pixels (14-18%) and low average correlation values for MaxNDVI occurred also for the summer Laptev sea ice area and adjacent land area. The highest proportion were, however, found for the Barents land area and Chukchi Sea SIA.

Positive correlations (high/low sea ice area – high/low TI-NDVI) were found for Eastern Taymyr for November to January (Figure A2; Sea ice in the East Siberian Sea to Beaufort Sea regions; January preceding to TI-NDVI value and November and December after).

The importance of sea ice regions for vegetation can switch from basin to basin throughout the year. For example, the Kara Sea tundra region MaxNDVI correlated with ESS SIA in summer and Barents and Svalbard SIA in April. The strong sea ice link of eastern to far eastern Siberia was also reflected in TI-NDVI correlation values (< -0.5). In the case of these highest values, the Beaufort SIA was relevant from January to June. This pattern switched to the Chukchi and to East Siberian Sea from July to November.

https://doi.org/10.5194/egusphere-2025-1358
Preprint. Discussion started: 7 May 2025


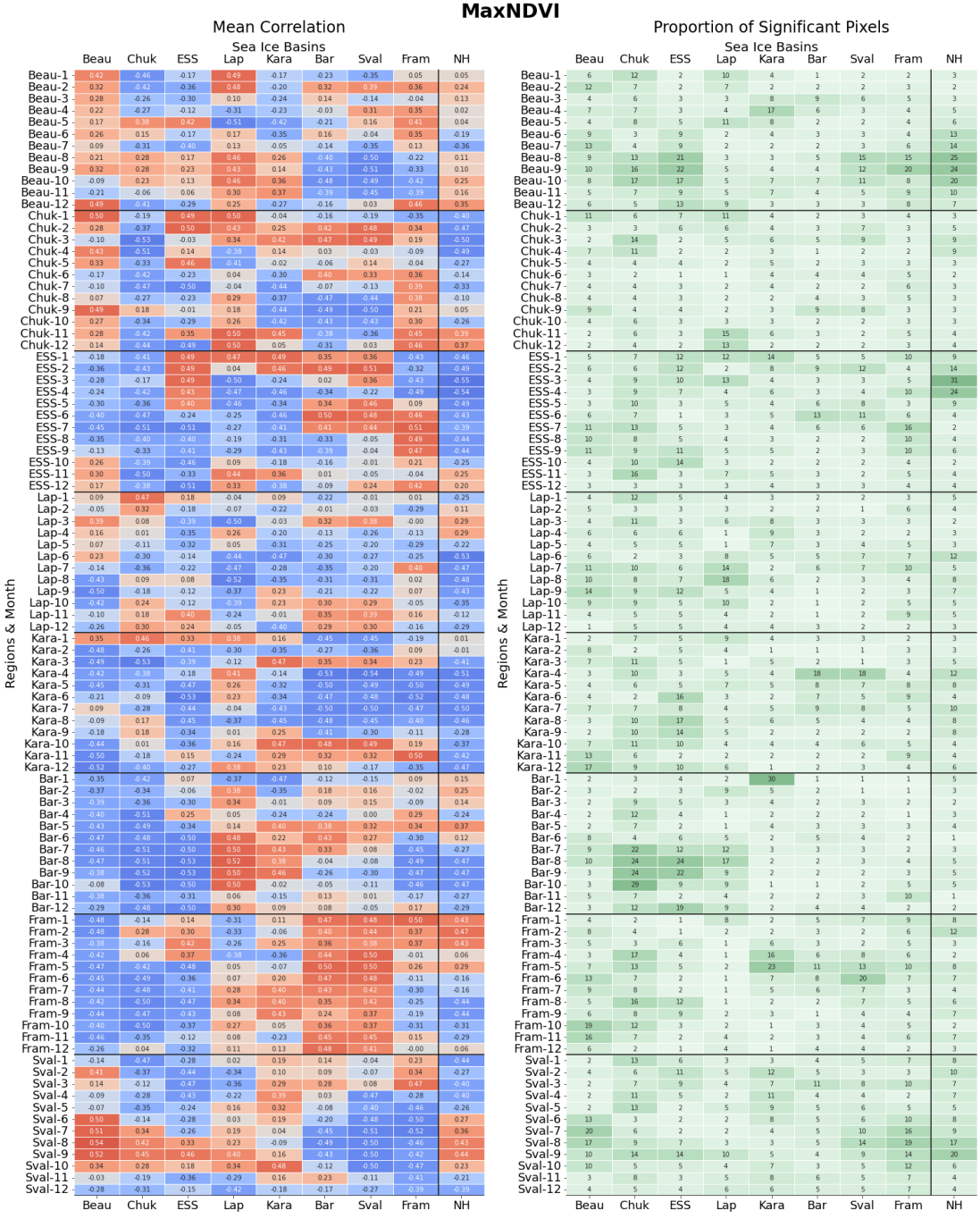


**Figure 5.** Significant correlations (95%) and proportion of significant pixels for sea ice area (by basin) versus MaxNDVI within CAVM regions (see Figure 1 for abbreviations and Table 4 for data sources).

https://doi.org/10.5194/egusphere-2025-1358
Preprint. Discussion started: 7 May 2025


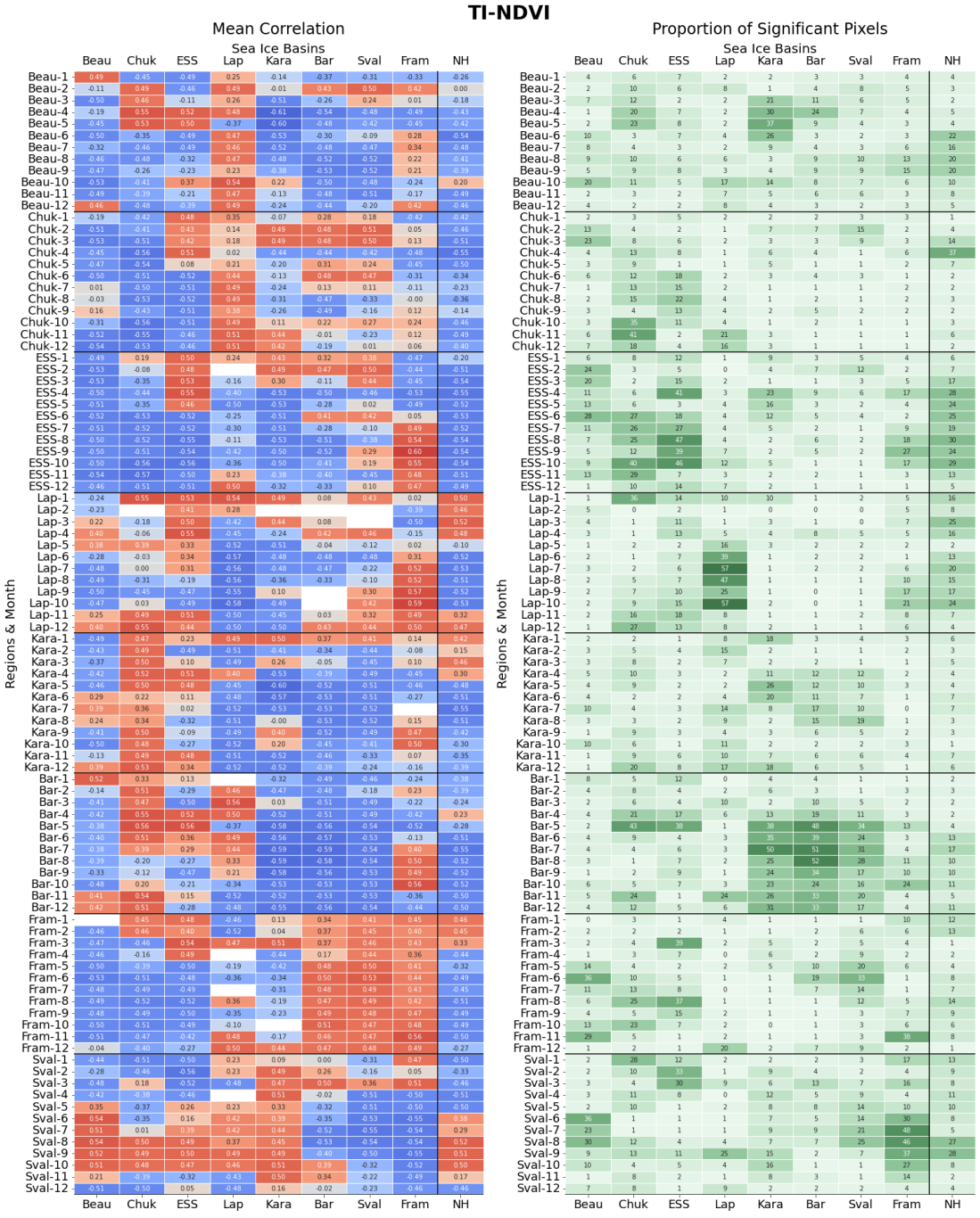


**Figure 6.** Significant correlations (95%) and proportion of significant pixels for sea ice area (by basin) versus TI-NDVI within CAVM regions (see Figure 1 for abbreviations and Table 4 for data sources).

https://doi.org/10.5194/egusphere-2025-1358
Preprint. Discussion started: 7 May 2025


Linkages for TI-NDVI could be also identified south of the CAVM boundary, specifically over Russia as well as Scandinavia (Figures A8, A10). June Fram Strait SIA correlated along the Norwegian coast. The Laptev Sea ice extent in July and August was linked to TI-NDVI in central Siberia.

### 3.2.3 Sea ice and SWE

March SWE and SIA correlations were partially negative and partially positive (Figures 7,A11, A13, A12, A14). Nevertheless, minimum and maximum values derived from samples of the same pairing (land subregion and sea ice basin) had mostly the same direction. Exceptions were SW Alaska for July (preceding year; lowest value for the Beaufort Sea and highest for Fram Strait Sea), Yamal for April (preceding year; lowest for ESS and highest for Kara Sea) and SE Taymyr for February (lowest for Fram Strait and highest for ESS).

Lower than average sea ice conditions in February linked to higher SWE in March across many parts of Siberia and SW Alaska (Figure A11). Negative correlation values are found for Chukchi Sea and Fram Strait SIA conditions across most CAVM regions. For March, Fram Strait linkages were most dominant (Figure A12). Parts of Alaska exhibited a significant negative correlation with October and November Fram Strait SIA and positively for December to February Beaufort Sea SIA. December to March SIA in the Chukchi Sea correlated negatively with SWE in Eastern Siberia. Beaufort and Chukchi SIA correlated negatively with parts of central Siberia for almost all months, except March. Positive correlations for parts of western to central Siberia were found for the Kara Sea SIA for October, November and January. Thus, over this region, larger sea ice extent in autumn linked to higher SWE in March.

SIA in the Chukchi, East Siberian, Kara Sea, Fram Strait and the NH average showed the highest proportions of significant correlations with SWE in tundra areas (Figure 7). The NH average SIA across the cold season correlated significantly with SWE specifically in Eastern Siberia, Laptev coast and Kara Sea regions (Figures A12 and A14). Barents and Svalbard Sea SIA had comparably fewer significant correlations with March SWE (Figure 7). The land area adjacent to the Chukchi Sea had high SWE when SIA in the Chukchi and Beaufort Sea was low in the previous year Summer/Autumn. The Kara Sea tundra regions had higher March SWE when the NH and Fram Strait average SIA was low in Jan/Feb and when Fram strait SIA was low in Autumn (but also high SWE when high SIA in Kara and Beaufort Sea region as well as NH average in early winter).

https://doi.org/10.5194/egusphere-2025-1358
Preprint. Discussion started: 7 May 2025


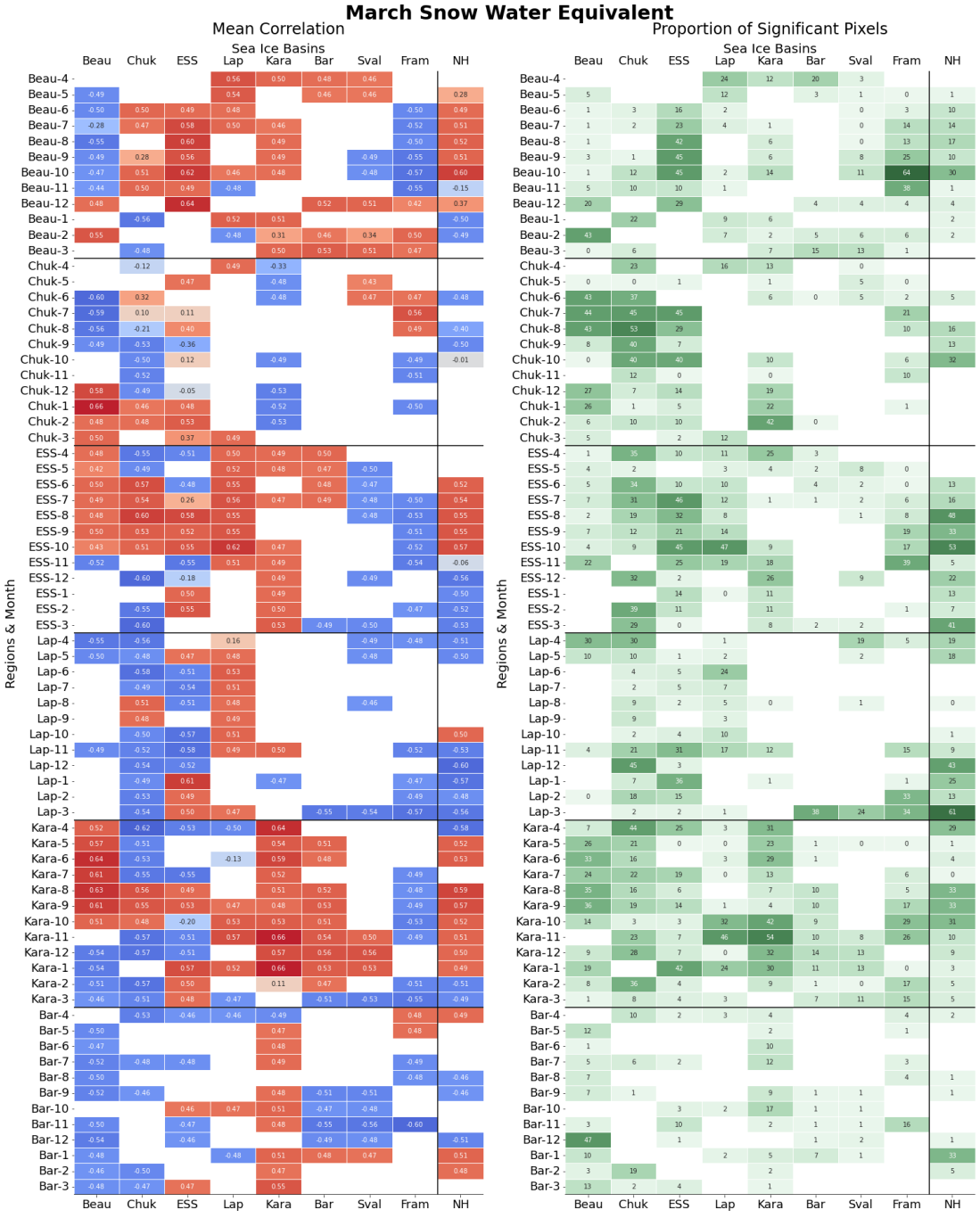


**Figure 7.** Significant correlations (95%) and proportion of significant pixels for sea ice area (by basin) versus snow water equivalent within CAVM regions (see Figure 1 for abbreviations and Table 4 for data sources). Months 4-12 represent preceding year.

https://doi.org/10.5194/egusphere-2025-1358
Preprint. Discussion started: 7 May 2025


## 4 Discussion

### 4.1 Trends

Li et al. (2023) demonstrated issues with orbital drift in AVHRR/GIMMS. Our results and Frost (2025) confirm differences in the Max-NDVI trend results compared to MODIS and Landsat. Trend patterns of MODIS and Landsat do, however, largely agree (Figure A1), confirming the utility of the MODIS dataset chosen for our study.

Bhatt et al. (2017) reported a declining trend of TI-NDVI and browning for Yamal based on AHVRR/GIMMS, and this is also reported for Western Siberia including parts of Yamal for 1982-2019 by Druckenmiller et al. (2021). MODIS and Landsat based trend analyses starting 2000 show, however, increasing values (Figure A1).

The regions with strongest positive TI-NDVI trends for 2000-2019 (Figure 3) were the Taymir peninsula and parts of northern mainland Canada. These regions coincide with areas of increased solar absorption trends (1998-2015) as identified previously with reanalyses data (Letterly et al., 2018) as well as regions with decreasing trends in frozen days during spring time (2000-2019, Figure A1).

The SWE trend investigation by Pulliainen et al. (2020) focused on March for 1980-2018. The study also found statistically significant trends of increasing snow water equivalent (SWE) over regions both in Western Siberia and Russian Far East. In contrast, Pulliainen et al. (2020) reported decreasing trends of SWE over North America, notably over regions surrounding the Hudson bay as well as areas adjacent to the Beaufort sea. The latter also agrees with our results based on the years 2000-2018.

### 4.2 Correlations

TI-NDVI correlations were more negative for May and June sea ice extent in Northwestern Russia than with MaxNDVI, with the strongest link being with the adjacent Kara Sea. This early summer pattern agrees with monthly NDVI regional analyses in Macias-Fauria et al. (2012) for this region, who identified May as a month of importance for the period 1992-2005. In our results, April appears more relevant for the more recent analyses period (2000-2019). This might relate to continuous decline of sea ice extent across all months. However, the proportion of significant correlations was only 18% (Figure 5). The partial linkage of NDVI on Svalbard with the surrounding SIA found by Macias-Fauria et al. (2017) and Karlsen et al. (2024) was confirmed in our analysis. The months selected by Karlsen et al. (2024) for sea ice area averaging (May to September) showed the highest proportion of significant values (up to 25%) in the case of Svalbard SIA. But our results show that also more distant basins showed significant correlations with Svalbard NDVI (Figure 6). These include the neighboring Fram Strait (negative correlation, up to 48% significant) as well as the Beaufort Sea area (positive correlation, up to 36% significant) in the case of TI-NDVI. The negative correlations of Svalbard NDVI-based variables with Fram Strait sea ice extent also agree with Macias-Fauria et al. (2012), who attributed them to the dynamics of the North Atlantic Oscillation driving warm air advection and sea

https://doi.org/10.5194/egusphere-2025-1358
Preprint. Discussion started: 7 May 2025


ice decline in the wider region.

Regions on land with significant correlations with sea ice are to some extent similar for ground temperature and NDVI (e.g. Figures A3 and A5). Specifically, results for Eastern Siberia show significant correlations among these parameters. In the case of ground temperatures, we report linkages with more distant basins then compared to NDVI, where the adjacent basins show the highest correlations across the Arctic (Figure 9). The latter applies specifically to the summer months July and August. In our study, MaxNDVI more strongly reflects sea ice changes than previously reported (Bhatt et al., 2021). Bhatt et al. (2021) reported -0.07 and -0.33 for the CAVM zones of Northern Eurasia and North America. Negative correlations were stronger (mostly <-0.4) in our results, which are based on MODIS instead of AVHRR/GIMMS. Our analysis cannot confirm the stronger negative correlations for MaxNDVI over North America as compared to Siberia identified in Bhatt et al. (2021), as Bhatt et al. (2021) used 50% sea ice concentration timing (which can represent differing months) and this study compiled correlations for specific months.

Both spring and summer sea ice extent were found to play a role for NDVI derivatives but with differing spatial patterns. Whereas Summer sea ice conditions showed low negative correlations with specifically tundra regions across all Arctic coasts, this was less pronounced for winter sea ice.

The regions identified as areas with strong positive trends in TI-NDVI (Figure 3) show distinct sea ice correlation patterns compared to other areas. Correlations are positive for several months in autumn and early winter, meaning that higher sea ice extents coincide with higher TI-NDVI in the following summer. In Northern Canada, the highest correlations were found vs. the Kara Sea ice extent, and in Taymyr these were found for the Chukchi Sea (Figures A9 and A10). Comparably high positive TI-NDVI correlations (with 15-21% significant values) also occurred for November and December Laptev SIA and the Chukchi Sea tundra region. So far, only preceding and temporally coincident sea ice conditions with the vegetation growing season have been discussed in the literature. Our results indicate that regional patterns which drive processes reflected in NDVI (such as warmer summers), also expressed in high absorption of solar radiation as represented in reanalysis data (see trend discussion in section 4.1) may regionally turn into colder than average conditions towards autumn, leading to earlier sea ice formation.

The use of predefined sea ice basin extents in our study resulted in broader investigated areas than in Bhatt et al. (2013) and also in exclusion of some regions. The latter specifically applies to the Canadian Arctic Archipelago, Baffin Bay, and Davis Strait, for which Bhatt et al. (2013) found comparably high correlations of open water extent with TI-NDVI on adjacent land area. The boundaries of the other sea ice basins, however, mostly agree with those used by Bhatt et al. (2013), but sub-basins for Barents, Kara and Chukchi Sea were merged in our analysis. The significant correlations for the East Siberian Sea and Chukchi Sea identified in Bhatt et al. (2013) agree with results from our study. Similar correlations were found in our study for the Laptev Sea summer months and adjacent land area (appr. 0.3 $R^2$; Bhatt et al. (2013) 0.31). Different results were

https://doi.org/10.5194/egusphere-2025-1358
Preprint. Discussion started: 7 May 2025


obtained for the Kara Sea. $R^2$ values higher than 0.3 were identified for MODIS-derived TI-NDVI (2000-2019), compared to 0.06/0.07 based on the AVHRR TI-NDVI (1982-2008) reported in Bhatt et al. (2013). This might be due to the different observation period, indicating recent changes in this region, or to the reported issues with the AVHRR dataset (Li et al. (2023)).

Bhatt et al. (2013, 2021) suggested that the linkage between sea ice and NDVI indices becomes weaker with advancement of sea ice decline. The patterns identified with data covering 2000-2019 are however similar to results for longer period based on AVHRR. Similarly, Karlsen et al. (2024) reported a recent rapid increase in Svalbard tundra productivity, evidenced as the integrated MODIS-NDVI from the phenologically-based onset (O) to the Peak (P) of the growing season (OP NDVI). This trend was strongly related to the recent increase in growing season temperature and in agreement with the last decade transition from perennial sea ice to absent sea ice around the eastern part of the Svalbard archipelago. Significant negative correlations were also found in our study for Svalbard (Figures 5 and 6).

The specific TI-NDVI correlation spatial patterns identified by Dutrieux et al. (2012) for the Taymyr to eastern Siberian regions (decline of correlations with distance to coast, up to 300km, in June) can be partially confirmed. But this pattern cannot be observed for other months, specifically for the following ones, which show higher correlations with sea ice area in this region (Figure 6).

Significant correlations of TI-NDVI as well as MaxNDVI outside of the CAVM region were also found for the taiga biome, both in Eurasia (including Scandinavian mountain ranges) and Northern America. Sea ice key regions were identified for March SWE (Figure 9). Specifically, the Fram Strait and Chukchi Sea variations are reflected in SWE across the Arctic, including Western Siberia.

The importance of sea ice for Northern Eurasian snow conditions reported by Park et al. (2013) based on modeled snow depth for 1979-2006 can be confirmed for our analysis period 2000-2019. De-trending leads, however, to insignificant results for eastern Siberia. The importance of the Chukchi sea ice conditions for SWE across Alaska reported by Alexeev et al. (2016) for 1991-2008 were also confirmed by our results. Significant correlations were found for the Chukchi Sea and East Siberian and Laptev Sea region, which supports the link between Chukchi Sea ice and SWE variations in the Siberian Far East suggested by Pulliainen et al. (2020). Pulliainen et al. (2020) noted drastic snowfall events as a results of loss of sea ice in the adjoining Chukchi Sea during the last two years of the study period.

High negative correlations of March SWE with SIA in regions such as Northern Fennoscandia and Svalbard may have implications for wildlife and reindeer herding (Bokhorst et al., 2009; Vikhamar-Schuler et al., 2016). The increasing fragmentation of reindeer habitat in Svalbard (and possibly other areas around the circumpolar area), due to loss of sea-ice (SIA) as dispersal corridors (Peeters et al., 2020) will likely reduce the overall ‘effective’ area of suitable habitats (Pedersen et al., 2023).However, increased greening might compensate for this (Karlsen et al., 2024). Forbes et al. (2016) suggested a linkage of sea ice condi-

https://doi.org/10.5194/egusphere-2025-1358
Preprint. Discussion started: 7 May 2025


tions with rain-on-snow events for the Kara Sea adjacent land area, which impact wildlife, vegetation and ground temperatures. So far, reliable rain-on-snow detection based on satellite data has been limited to mid-winter and the number of documented large scale events is rather low Bartsch et al. (2023a). Linkages could thus not yet been proven based on satellite records.

Significant negative correlations with comparably distant sea ice basins, in addition to adjacent ones, were found for MAGT (Figure 9). This agrees with previous findings on observed cryosphere linkage antipodal to the North Pole for a further permafrost related parameter, active layer thickness (Sasgen et al., 2024). A high similarity with Arctic impact indices (from re-analysis data) was found for Central Siberian active layer thickness and the mass balance of the northern part of the Greenland ice sheet. Central Siberia MAGT also showed significant negative correlations with the Fram Strait SIA from January to March in our study (Figure A4). However, for permafrost, the Beaufort and East Siberian Seas appear to be the key regions. Sea ice in these basins showed significant correlations with land area, specifically in autumn (Figure 9). This included regions in Siberia. In case of the Beaufort Sea SIA, results indicate also a strong linkage with MAGT across the Canadian High Arctic for autumn. This could not be found for winter conditions (e.g. March, Figure 9).

Significant month-specific correlations of de-trended sea ice area time series were found across the year for all investigated land parameters. Further common satellite derived vegetation parameters such as Leaf Area Index (LAI) or phenology indicators (e.g. Park et al. (2016)) may provide additional insight into regional patterns. MaxLAI index trends show, however, similar patterns than MaxNDVI trends, exemplifiying the general linkage of LAI with NDVI (Figure 3 and Figure A1) and were thus not considered in the present study. An alternative parameter available from passive microwave satellite records is vegetation optical depth (VOD). Observed patterns have been shown to be relevant for recent changes in parts of the Canadian Arctic and Northeastern Siberia Watts et al. (2025). Phenology may also be represented through proxies such as snow extent or freeze-thaw (FT) datasets. The representation of the transition periods in satellite derived FT records is, however, challenging (Bartsch et al., 2025b).

The presented dataset provides information on potential linkages and thus a baseline for future studies on common drivers of essential climate parameters and dependencies across the Arctic. The consideration of Arctic change indices as applied by Sasgen et al. (2024) for glacier mass balance and permafrost active layer thickness may support such analyses.

## 5 Conclusions

Significant correlations of sea ice with satellite-based terrestrial variables across the Arctic are reported in this study. The importance of certain sea ice basins and timing differed between permafrost ground temperature, vegetation indices, and snow water equivalent. Autumn (incl. October and November) and mid-winter (incl. February, March) were most relevant for both investigated cryosphere-related parameters permafrost temperature and March snow water equivalent (used in here as a proxy

https://doi.org/10.5194/egusphere-2025-1358
Preprint. Discussion started: 7 May 2025


for maximum).

NDVI analyses confirm previous studies for the CAVM/tundra zone. Added value is, however, provided through inclusion of areas outside the tundra region. Areas with significant correlations extend into the boreal forest biome specifically across Siberia. An additional aspect was added through consideration of succeeding SIA conditions. For example, summers with high MaxNDVI along the Laptev Sea are followed by high sea ice concentration in the Chukchi sea.

SWE analyses confirm previous modelling results. Chukchi Sea sea ice affects March SWE in adjacent land areas. Fram Strait SIA also has specific regional linkages (Kara sea adjacent tundra region). Previous studies were, however, confined to September sea ice extent. Our results show that cold season SIA is of relevance across several areas. March SWE correlates highest with January to March SIA.

Sea ice and MAGT were so far investigated for the entire Northern Hemisphere only. The MAGT variation analyses for separate regions revealed differences. For the CAVM zone, significant correlations are reported for the Kara and Laptev Seas, with respect to sea ice basins located eastwards and across the Arctic ocean. Strongest linkages between sea ice and MAGT were found for Svalbard and the Laptev Sea regions, but with distinct timing. Winter SIA in the proximity correlated strongly with the Svalbard unglaciated areas, whereas summer SIA correlated with the Laptev Sea coast.

In the case of ground temperatures, high significant correlations against SIA were found for more distant basins than for NDVI, where the adjacent sea ice basins are more relevant. Both distant and adjacent land area March SWE showed significant results. Although similarities were found between TI-NDVI and MaxNDVI, more significant correlations were observed for TI-NDVI. Both TI-NDVI and MaxNDVI are integrative parameters over the growing season. The inclusion of phenology-related indicators could provide additional information on vegetation-related aspects. The current dataset may provide a baseline for analyses of drivers and dependencies, including also reanalyses data.

*Data availability.* Trend and correlation datasets are available on ZENODO (Bartsch et al., 2025a, c).

https://doi.org/10.5194/egusphere-2025-1358
Preprint. Discussion started: 7 May 2025


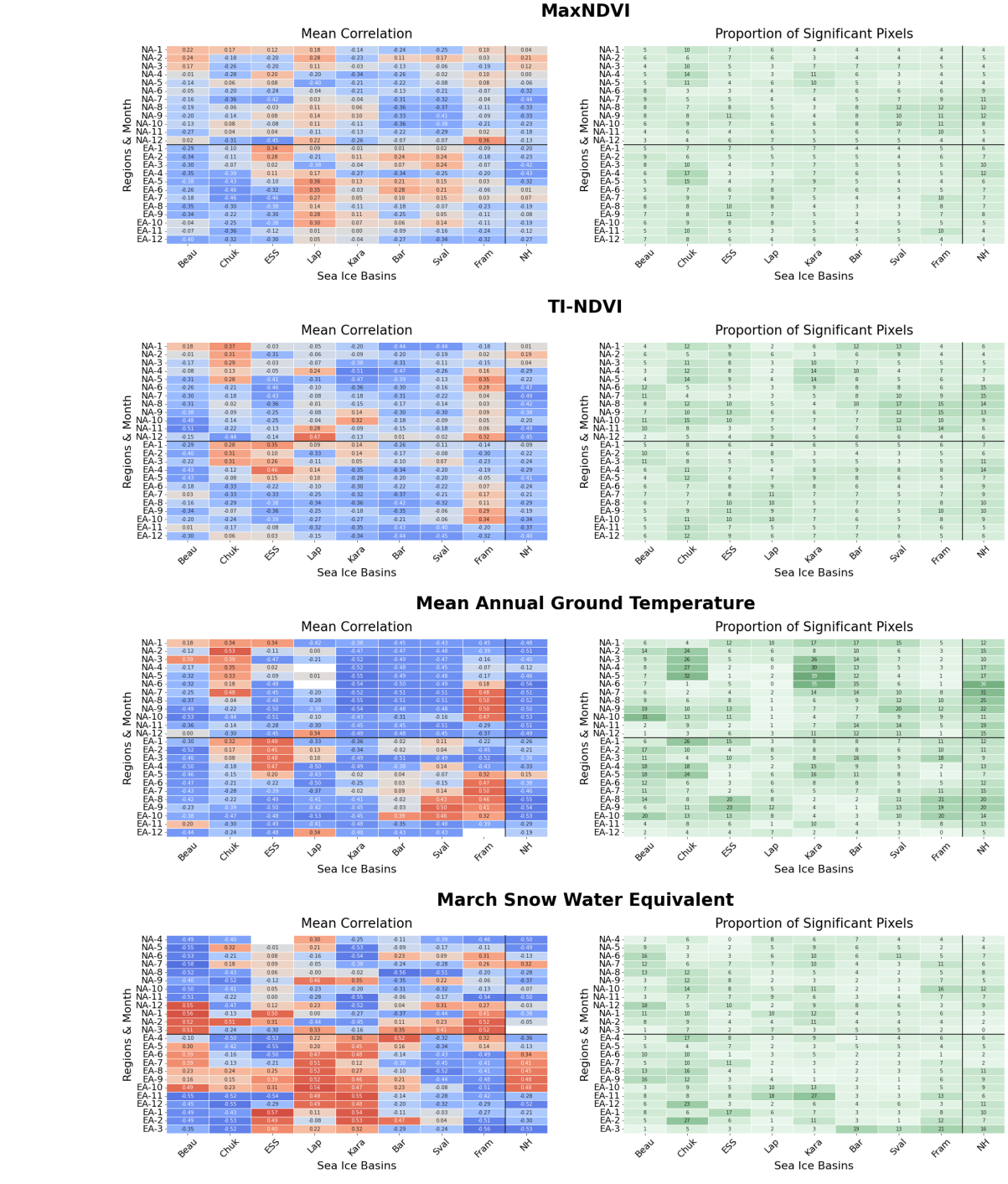


**Figure 8.** Significant correlations (95%) and proportion of significant pixels for sea ice area (by basin, see Figure 1 for abbreviations) versus mean annual ground temperature, MaxNDVI, TI-NDVI and snow water equivalent within North America (NA) and Eurasian (EA) north of 60°N. In case of SWE, months 4-12 represent preceding year. See Table 4 for data sources.

https://doi.org/10.5194/egusphere-2025-1358
Preprint. Discussion started: 7 May 2025


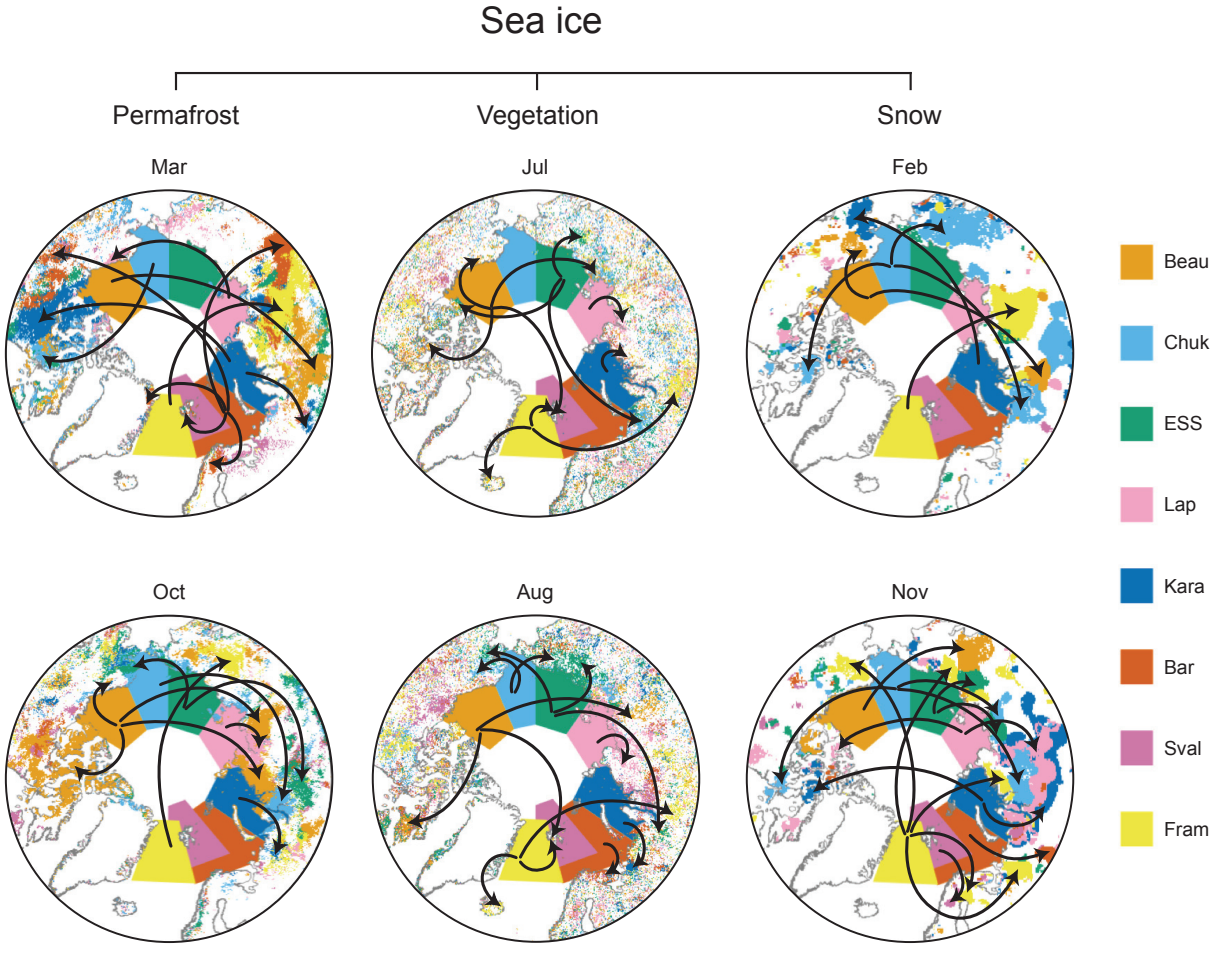


**Figure 9.** Areas with significant correlations for selected months and annotations (arrows) highlighting linkages. Permafrost - Mean annual ground temperature; vegetation top: MaxNDVI - maximum normalized difference vegetation index; vegetation bottom: TI-NDVI Time integrated Normalized difference vegetation index; snow: March snow water equivalent.

https://doi.org/10.5194/egusphere-2025-1358
Preprint. Discussion started: 7 May 2025


# Appendix A

## A1 Trends

**Table A1.** Satellite records used in selected published trend discussions for the Arctic

| **Comiso and Hall (2014), >64°N** | | **AMAP (2017), >60°N** | |
|---|---|---|---|
| **Parameter** | **Time period** | **Parameter** | **Time period** |
| Snow cover extent | 1981-2012 | Snow cover extent | 1981-2010 |
| Surface temperature Land and sea | 1981-2012 | Snow Water Equivalent | 1981-2014 |
| Sea ice extent | 1979-2012 | MaxNDVI | 1982-2015 |
| Greenland Mass balance | 2000-2012 | TI-NDVI | 1982-2015 |
| Albedo | 1981-2012 | | |
| Cloud cover fraction | 1981-2012 | | |

https://doi.org/10.5194/egusphere-2025-1358
Preprint. Discussion started: 7 May 2025


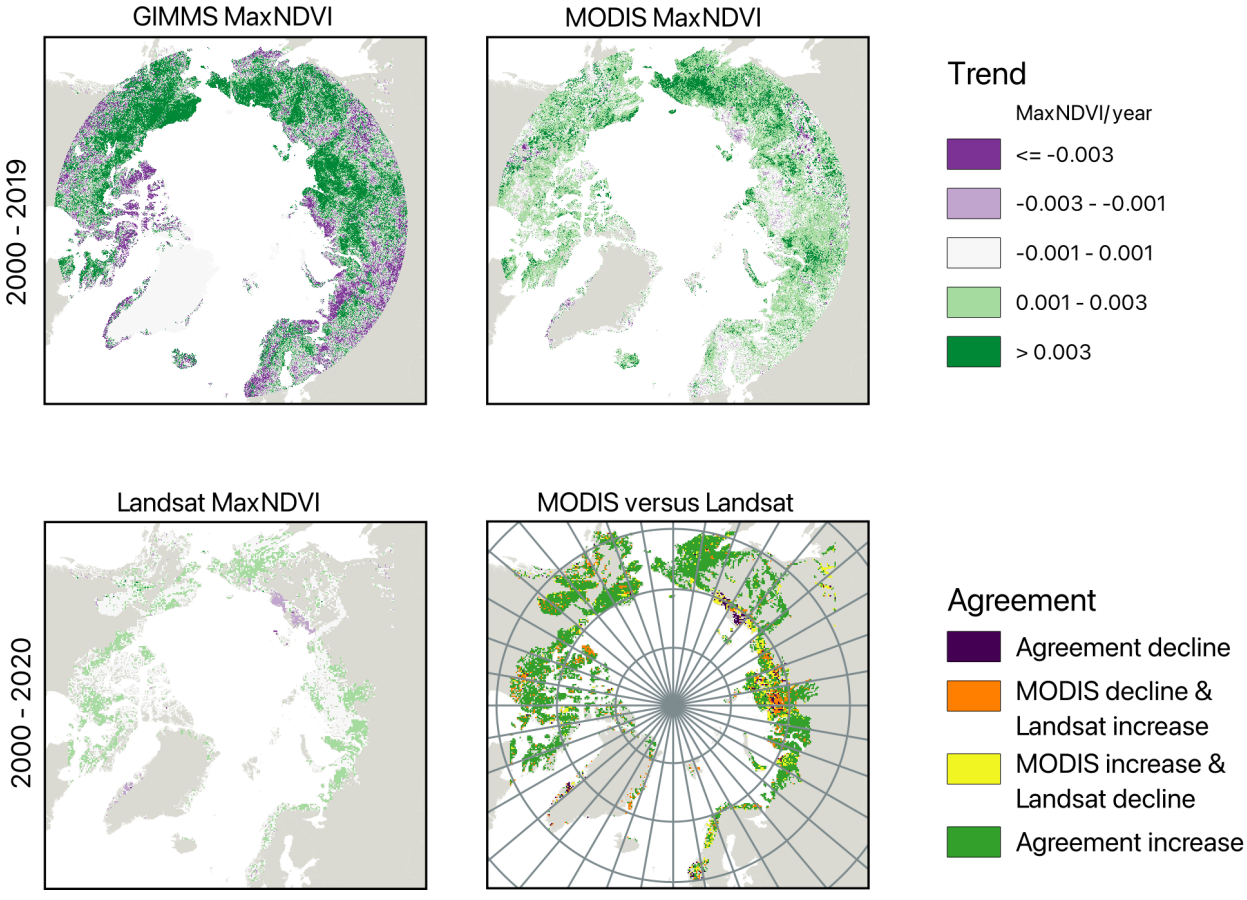


**Figure A1.** MaxNDVI trends for selected datasets: AVHRR (GIMMS), Landsat Mekonnen et al. (2021) and MODIS derived MaxNDVI trends for 2000-2019/2020.

https://doi.org/10.5194/egusphere-2025-1358
Preprint. Discussion started: 7 May 2025


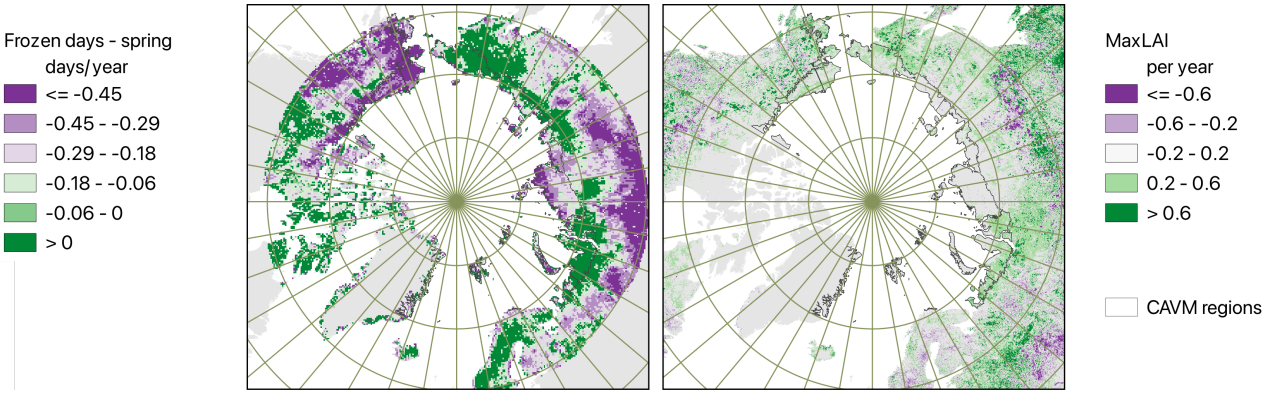


**Figure A2.** Trends in thawing period length derived from MEAsUREs (Kim et al., 2021) and Maximum Leaf Area Index based on MODIS (Source), 2000-2019.

https://doi.org/10.5194/egusphere-2025-1358
Preprint. Discussion started: 7 May 2025


**Table A2.** Averaged trends for North of 60°N for all analyses records. For specifications see Table 4.

| Dataset | Unit | Period | 2000? | Trend (per year) |
|---|---|---|---|---|
| **GlobSnow SWE March** | mm | 2000-2018 | | 0.014 |
| **Permafrost_cci MAGT (-2m)** | °C | 2000-2018 | | 0.065 |
| **MODIS MaxNDVI** | Unitless | 2000-2018 | | 0.0015 |
| **Landsat MaxNDVI (Arctic ecounits)** | Unitless | 2000-2020 | | 0.00071 |
| **MODIS TI-NDVI** | Unitless | 2000-2018 | | 0.012 |
| **MODIS MaxLAI** | m2/m2 | 2000-2019 | | 0.031 |
| **MEAsUREs Frozen days, spring period** | Days | 2000-2019 | | -0.18 |

https://doi.org/10.5194/egusphere-2025-1358
Preprint. Discussion started: 7 May 2025


## A2 Correlations

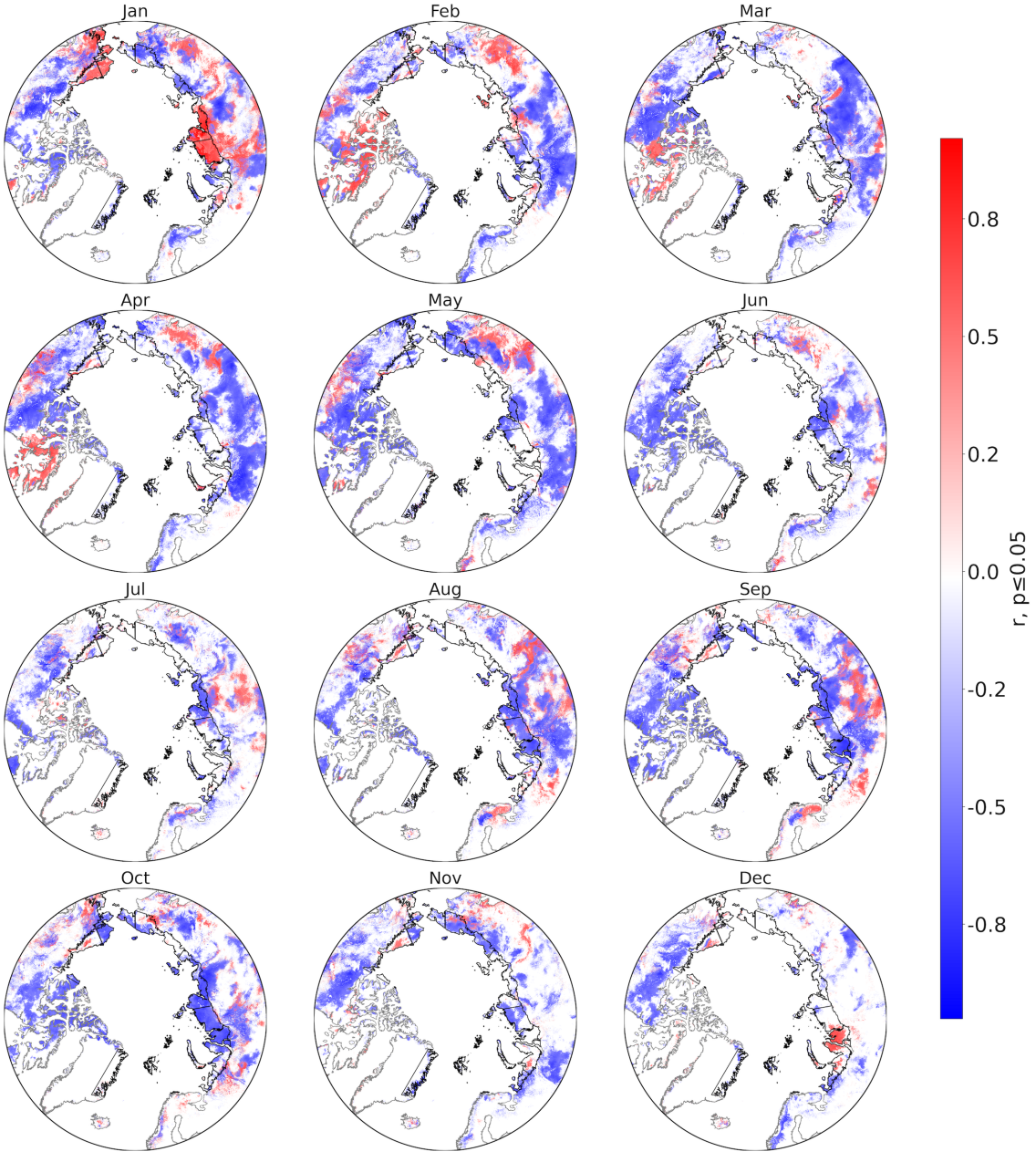


**Figure A3.** Minimum correlation of mean annual ground temperature at 2m depth (Obu et al., 2021a) and monthly, basin specific sea ice area (OSI SAF and EUMETSAT SAF On Ocean And Sea Ice, 2020), 2000-2019.

https://doi.org/10.5194/egusphere-2025-1358
Preprint. Discussion started: 7 May 2025


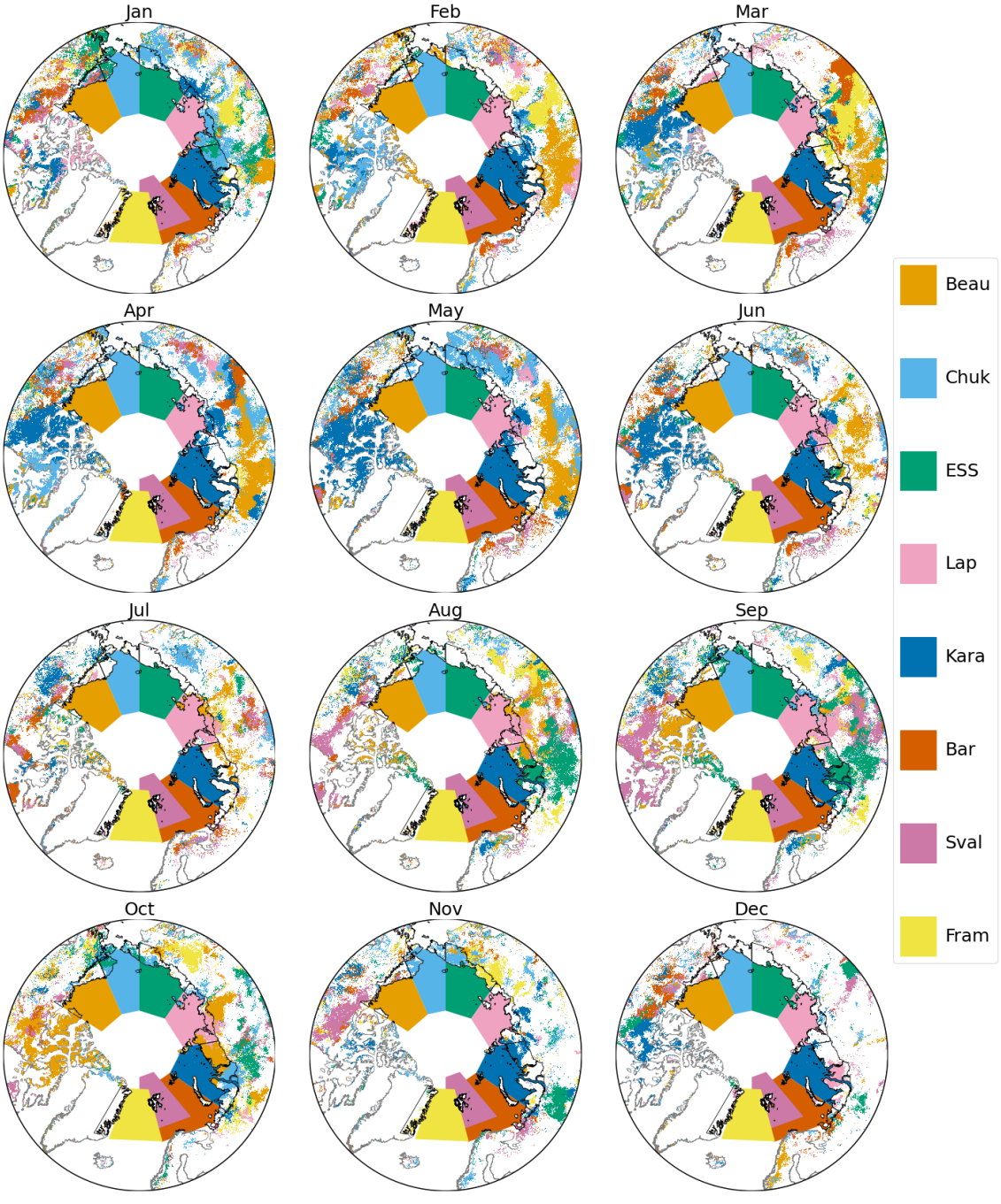


**Figure A4.** Area with significant minimum correlation of mean annual ground temperature at 2m depth (Obu et al., 2021a) with sea ice area and associated basin (OSI SAF and EUMETSAT SAF On Ocean And Sea Ice, 2020), 2000-2019. For actual basin extent and legend see Figure 1.

https://doi.org/10.5194/egusphere-2025-1358
Preprint. Discussion started: 7 May 2025


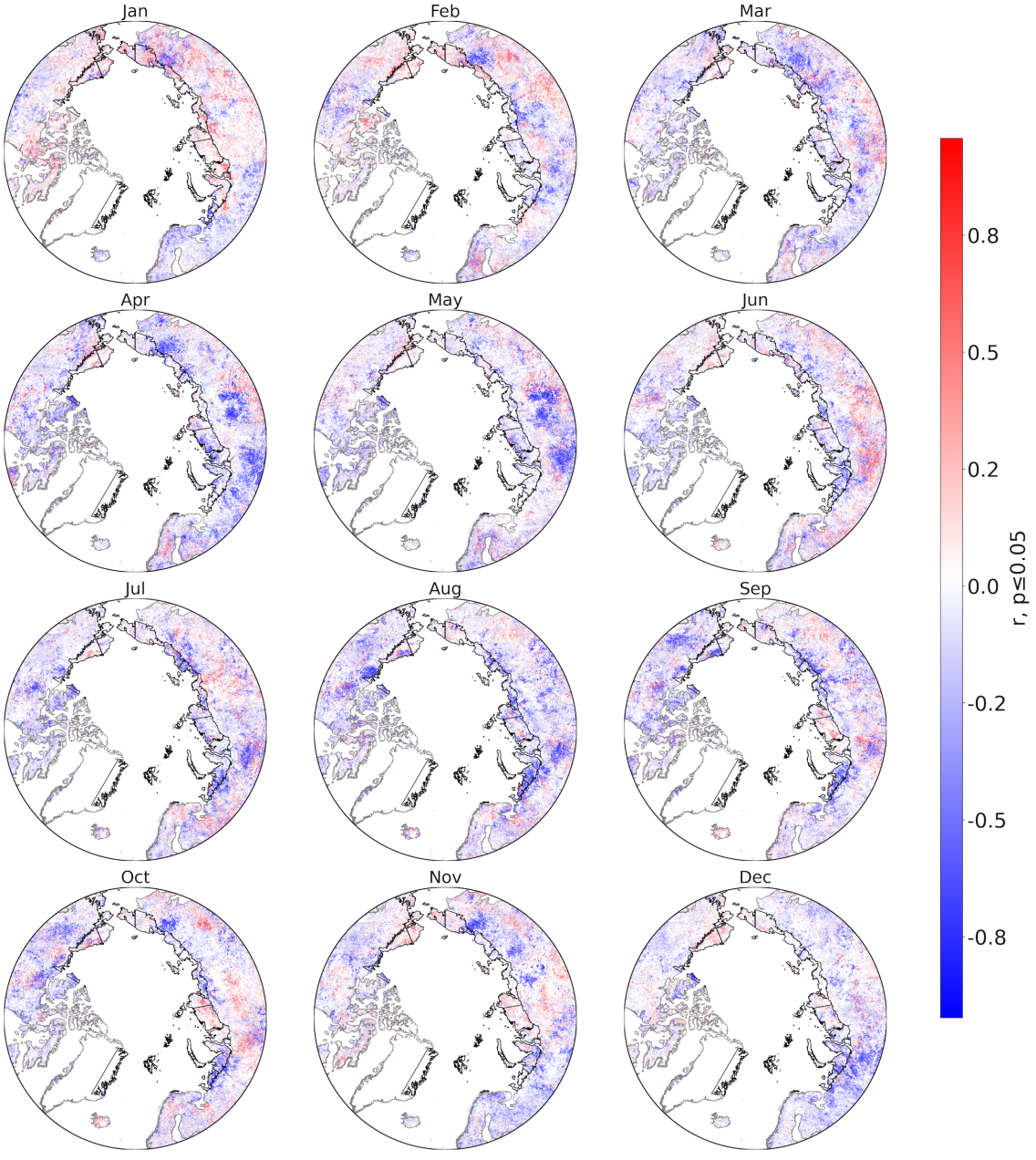


**Figure A5.** Minimum correlation of maximum NDVI (MODIS) and monthly, basin specific sea ice area (OSI SAF and EUMETSAT SAF On Ocean And Sea Ice, 2020), 2000-2019.

https://doi.org/10.5194/egusphere-2025-1358
Preprint. Discussion started: 7 May 2025


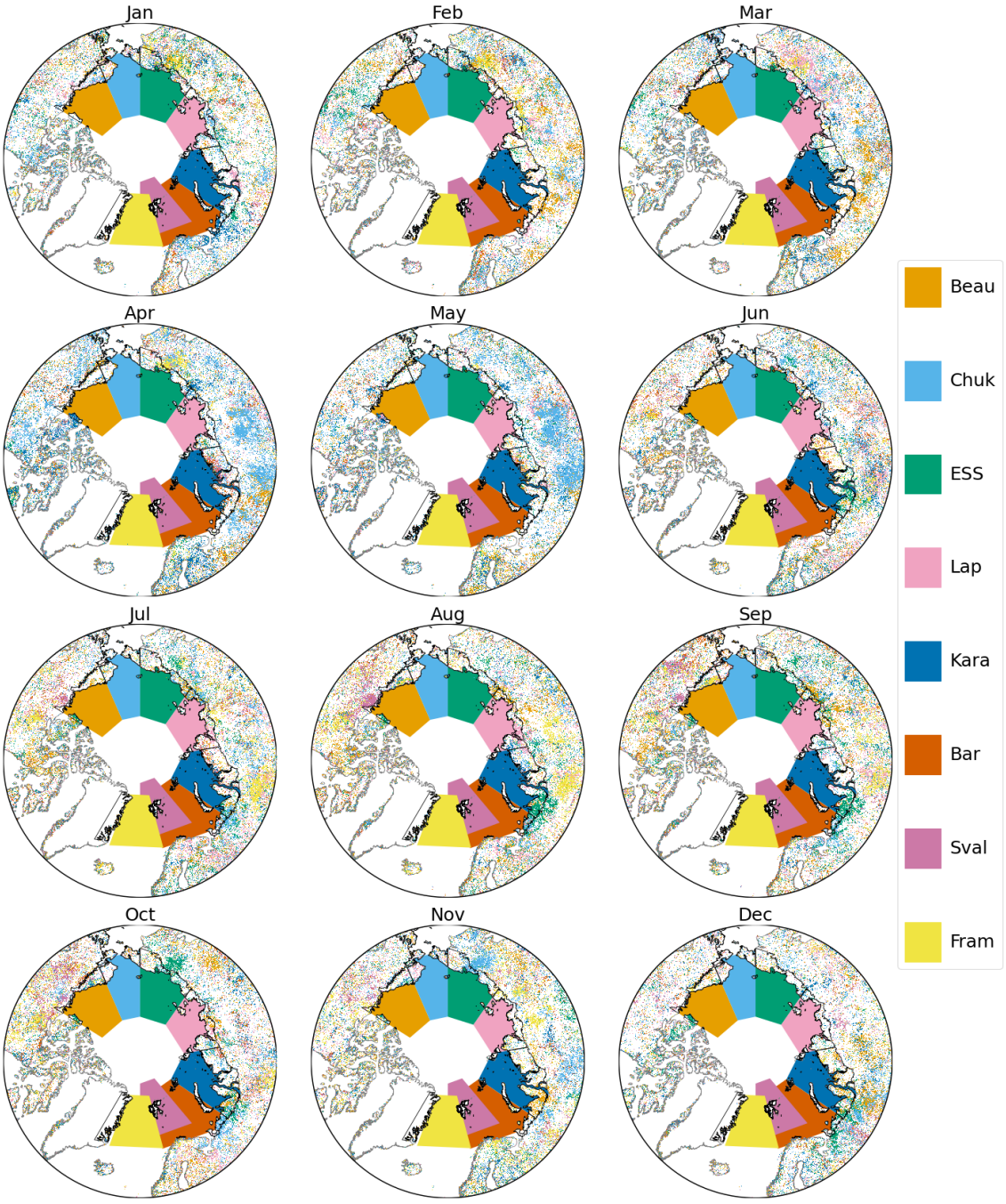


**Figure A6.** Area with significant minimum correlation of maximum NDVI (MODIS) with sea ice area and associated basin (OSI SAF and EUMETSAT SAF On Ocean And Sea Ice, 2020), 2000-2019. For actual basin extent and legend see Figure 1.

https://doi.org/10.5194/egusphere-2025-1358
Preprint. Discussion started: 7 May 2025


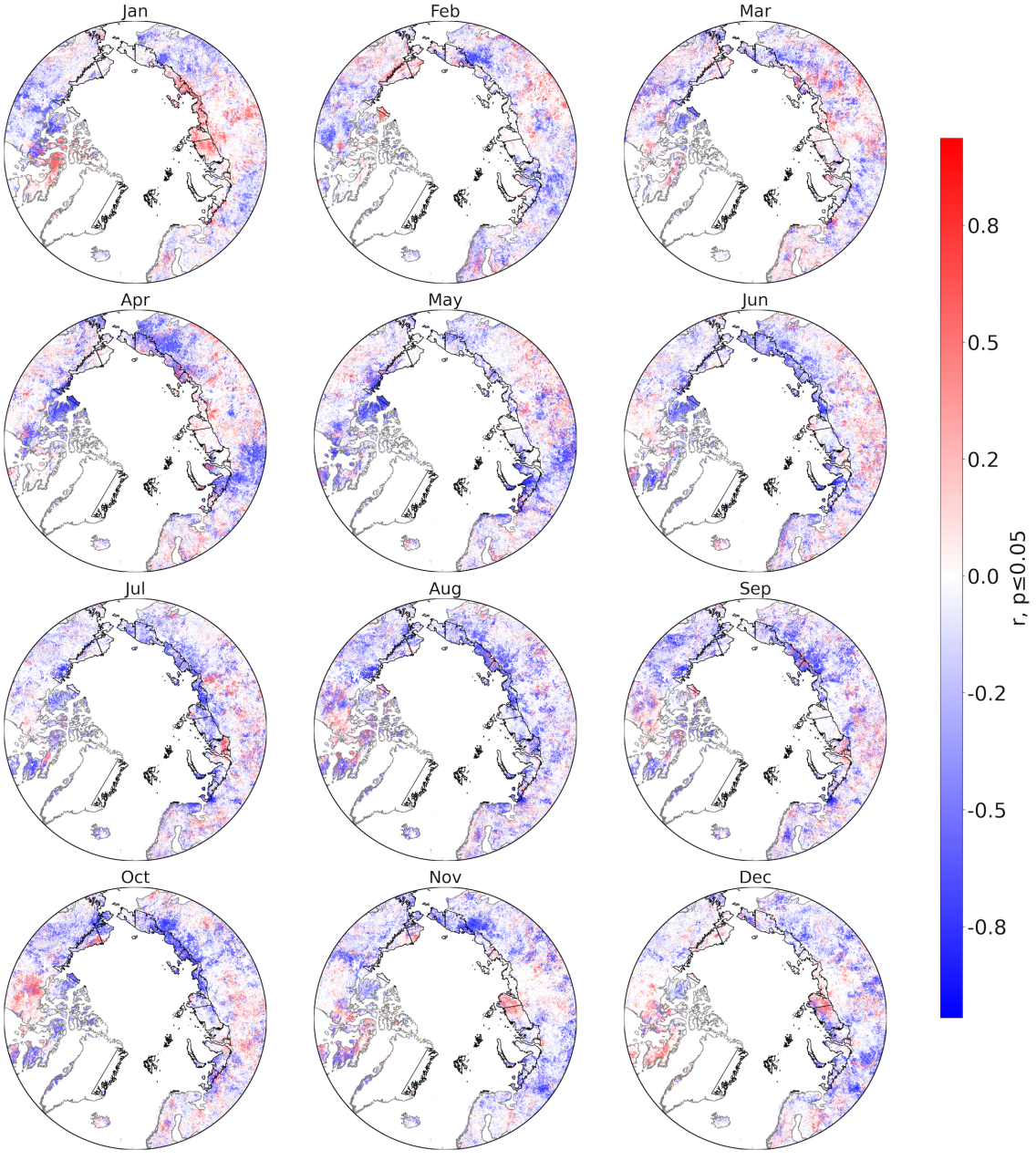


**Figure A7.** Minimum correlation of TI NDVI (MODIS) and monthly, basin specific sea ice area (OSI SAF and EUMETSAT SAF On Ocean And Sea Ice, 2020), 2000-2019.

https://doi.org/10.5194/egusphere-2025-1358
Preprint. Discussion started: 7 May 2025


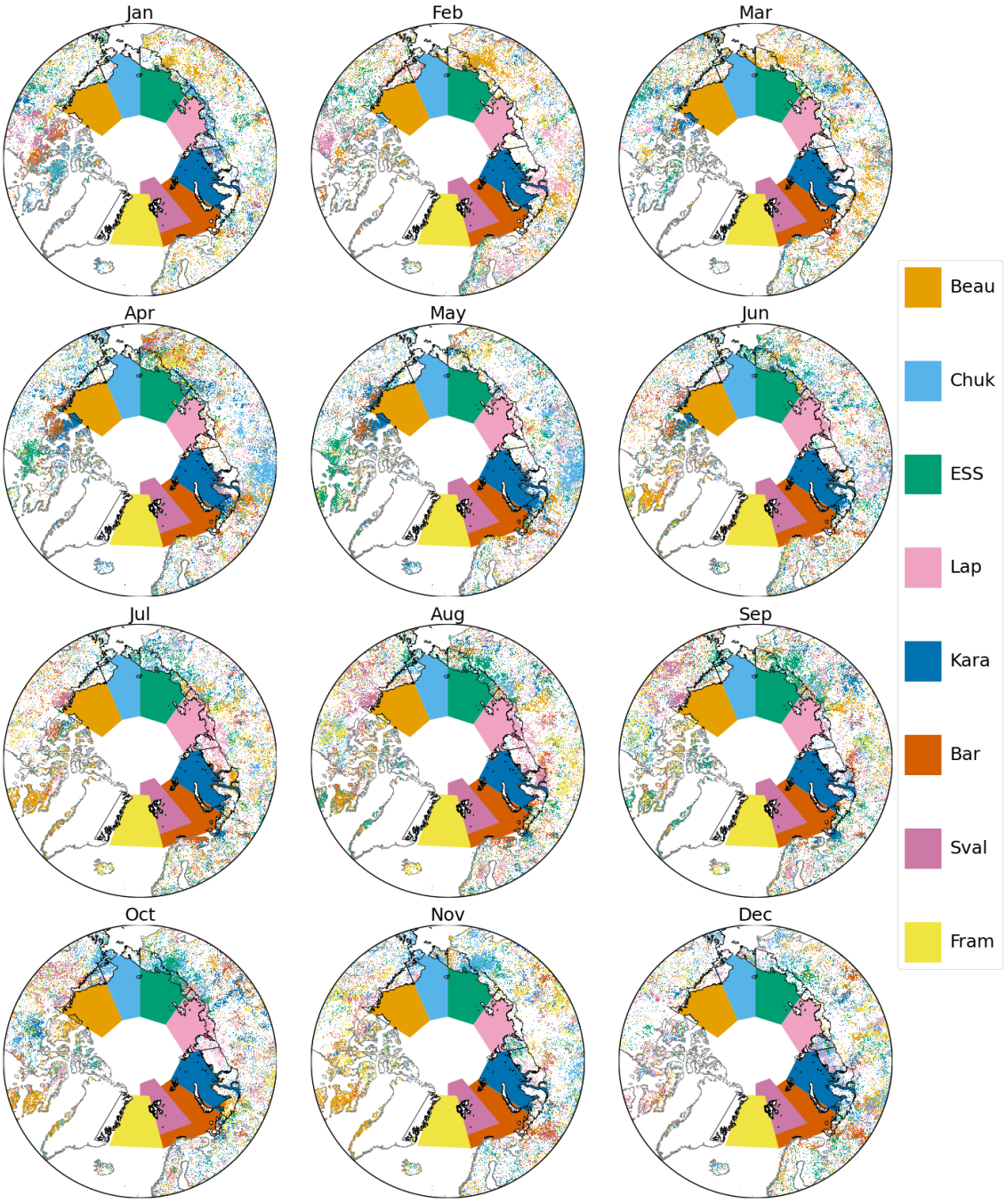


**Figure A8.** Area with significant minimum correlation of TI- NDVI (MODIS) with sea ice area and associated basin (source ESA CCI sea ice), 2000-2019. For actual basin extent and legend see Figure 1.

https://doi.org/10.5194/egusphere-2025-1358
Preprint. Discussion started: 7 May 2025


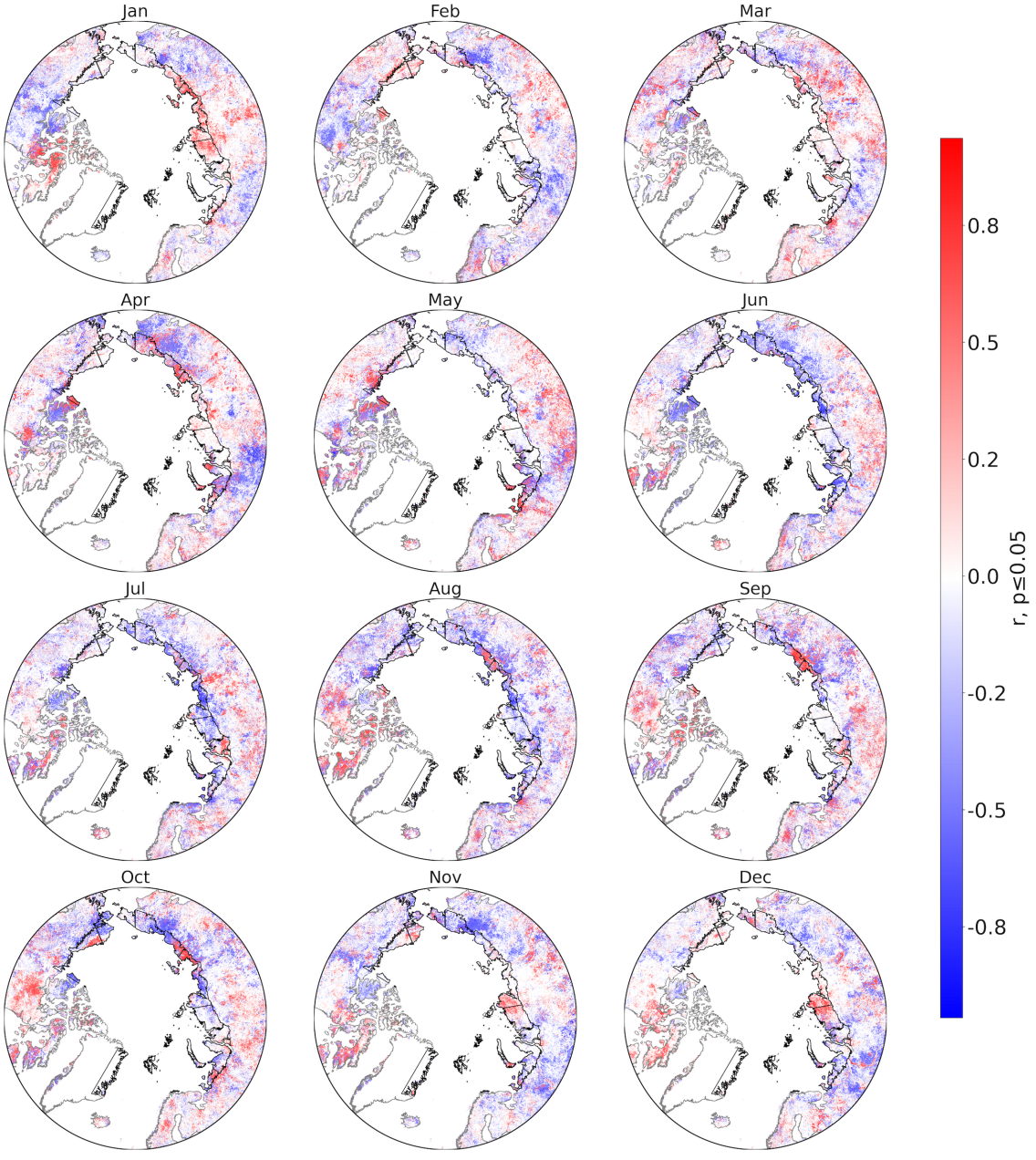


**Figure A9.** Maximum correlation of TI NDVI (MODIS) and monthly, basin specific sea ice area (OSI SAF and EUMETSAT SAF On Ocean And Sea Ice, 2020), 2000-2019.

https://doi.org/10.5194/egusphere-2025-1358
Preprint. Discussion started: 7 May 2025


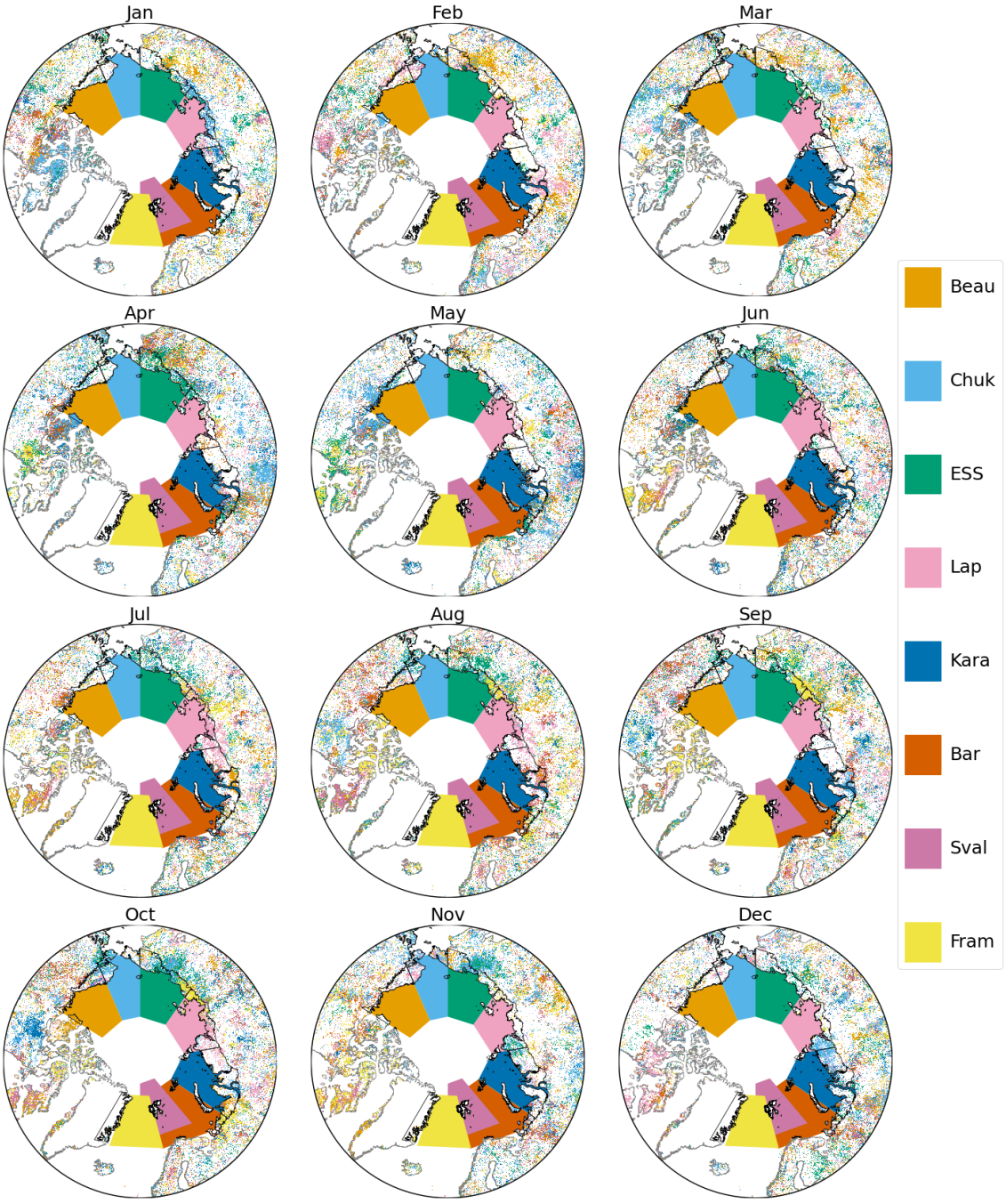


**Figure A10.** Area with significant maximum correlation of TI- NDVI (MODIS) with sea ice area and associated basin (OSI SAF and EUMETSAT SAF On Ocean And Sea Ice, 2020), 2000-2019. For actual basin extent and legend see Figure 1.

https://doi.org/10.5194/egusphere-2025-1358
Preprint. Discussion started: 7 May 2025


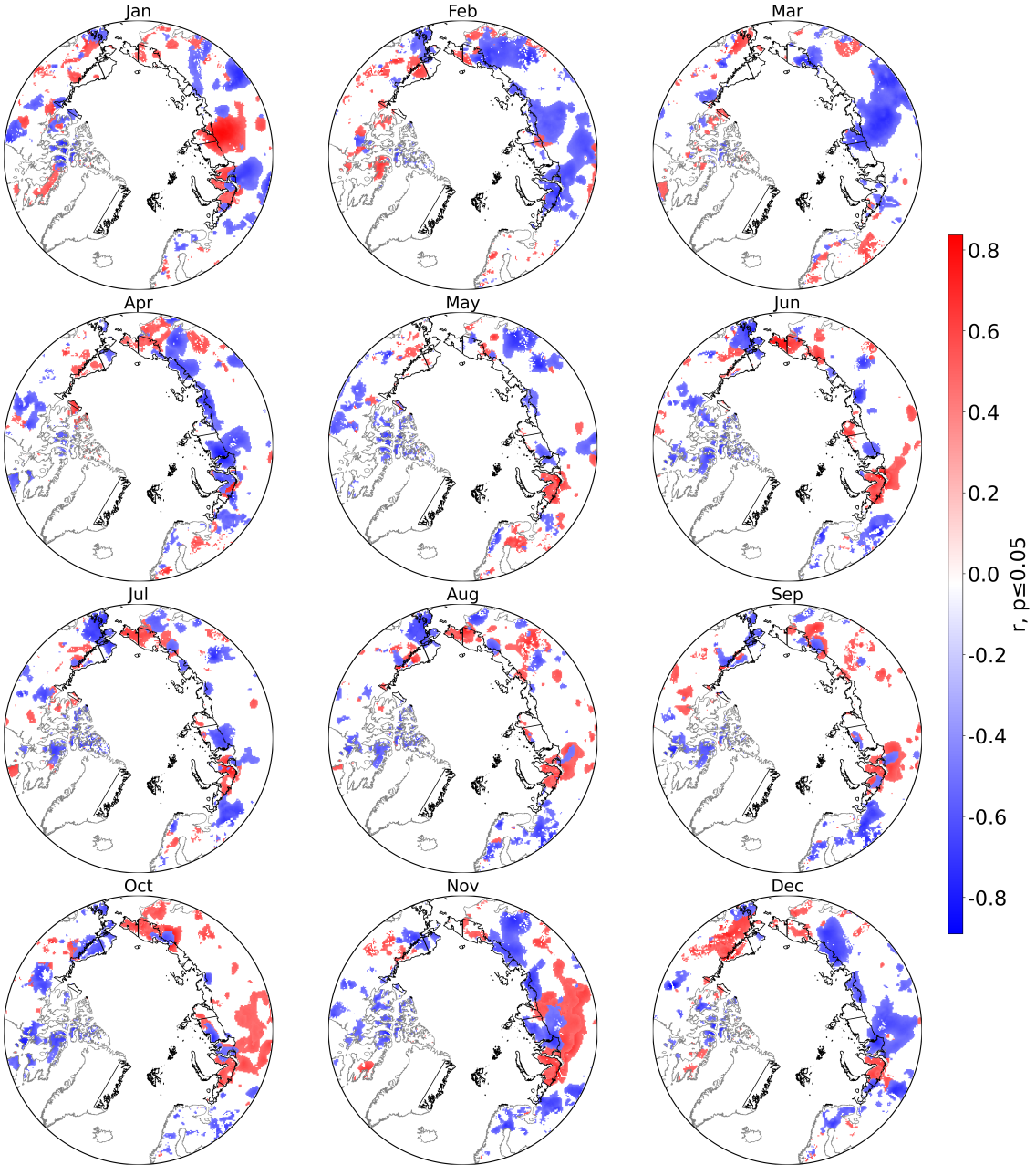


**Figure A11.** Minimum correlation of SWE (March) and monthly, basin specific sea ice area (OSI SAF and EUMETSAT SAF On Ocean And Sea Ice, 2020), 2000-2019.

https://doi.org/10.5194/egusphere-2025-1358
Preprint. Discussion started: 7 May 2025


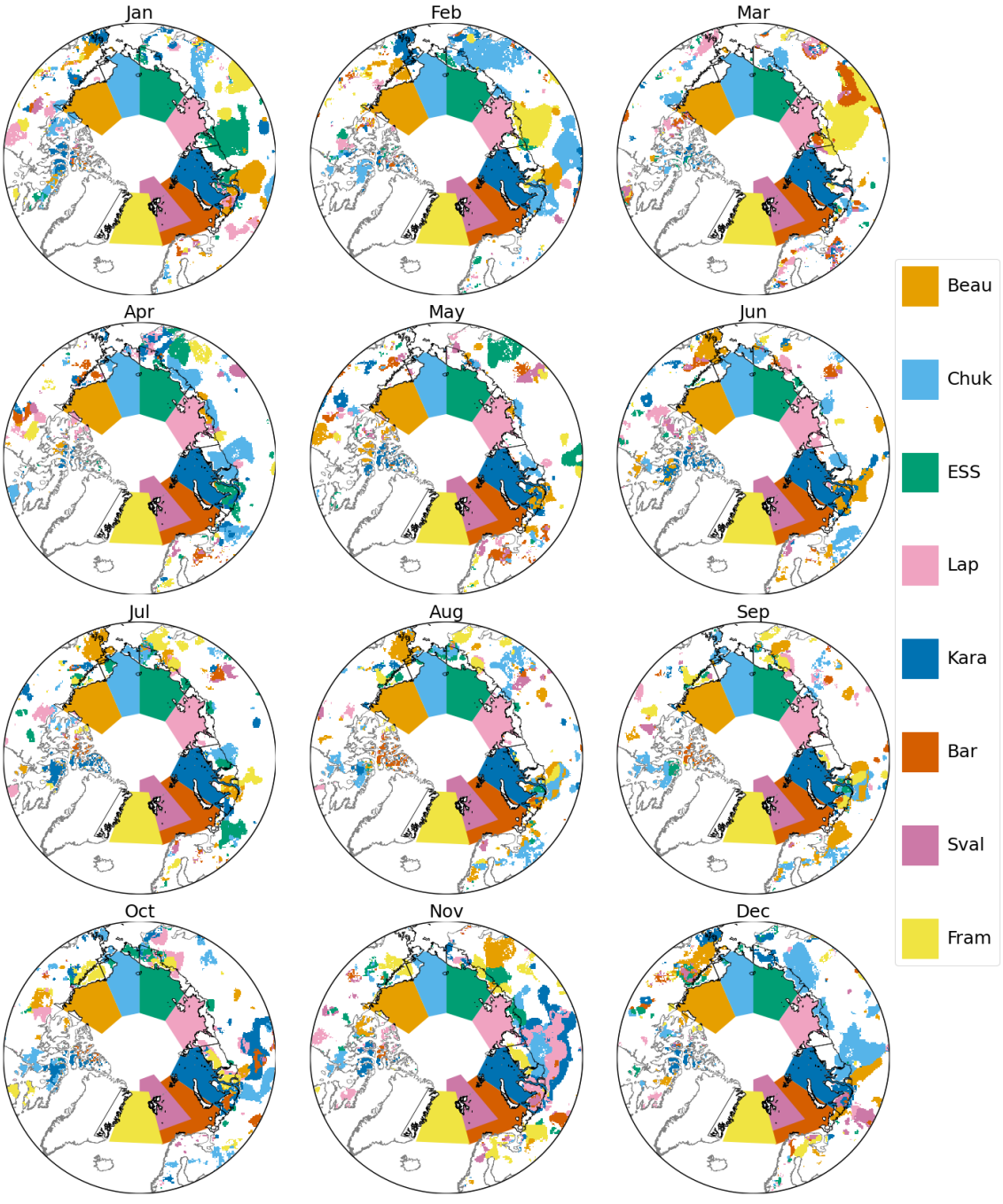


**Figure A12.** Area with significant minimum correlation of SWE (March) with sea ice area and associated basin (source ESA CCI sea ice), 2000-2019. For actual basin extent and legend see Figure 1.

https://doi.org/10.5194/egusphere-2025-1358
Preprint. Discussion started: 7 May 2025


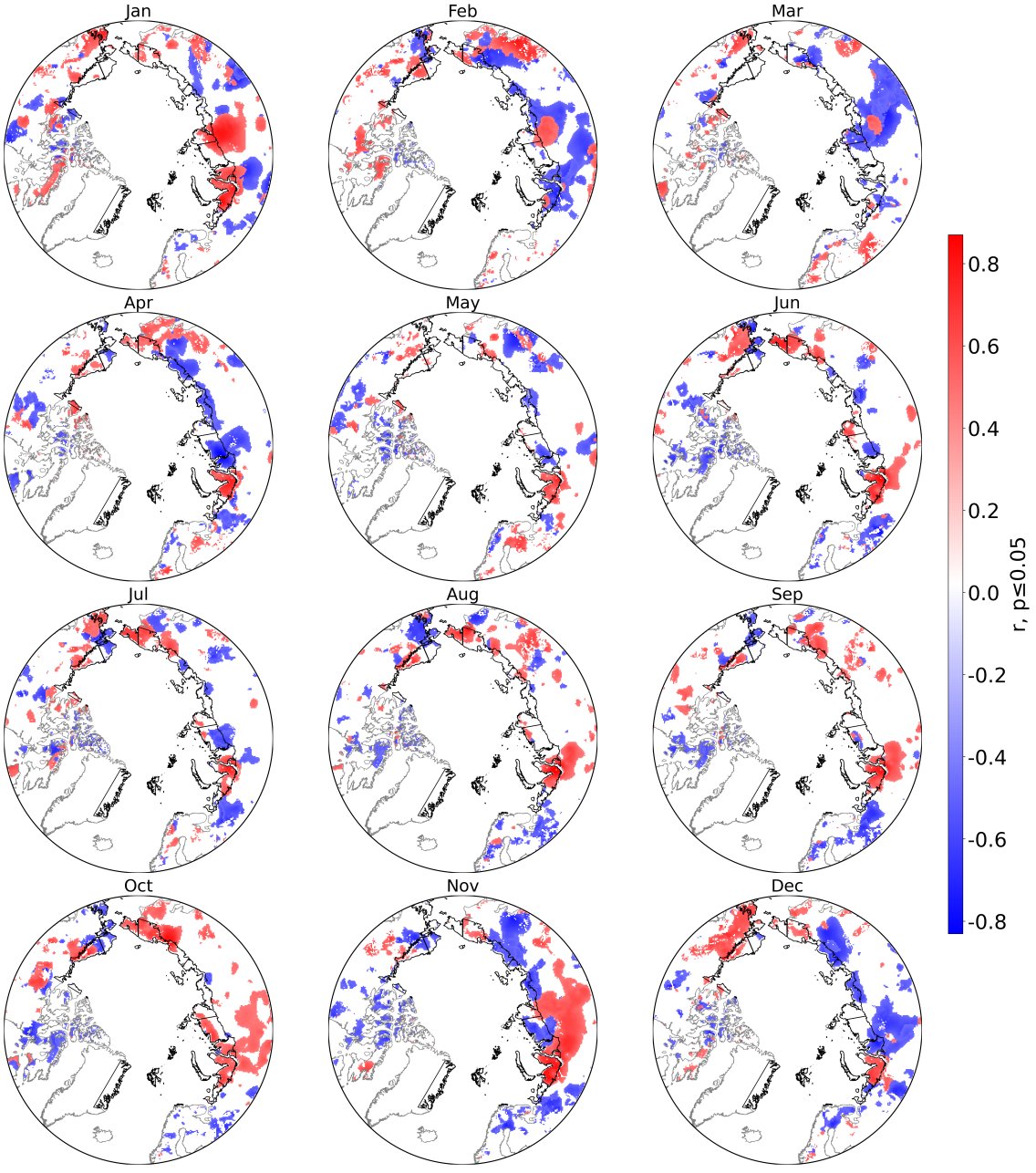


**Figure A13.** Maximum correlation of SWE (March) and monthly, basin specific sea ice area (OSI SAF and EUMETSAT SAF On Ocean And Sea Ice, 2020), 2000-2019.

https://doi.org/10.5194/egusphere-2025-1358
Preprint. Discussion started: 7 May 2025


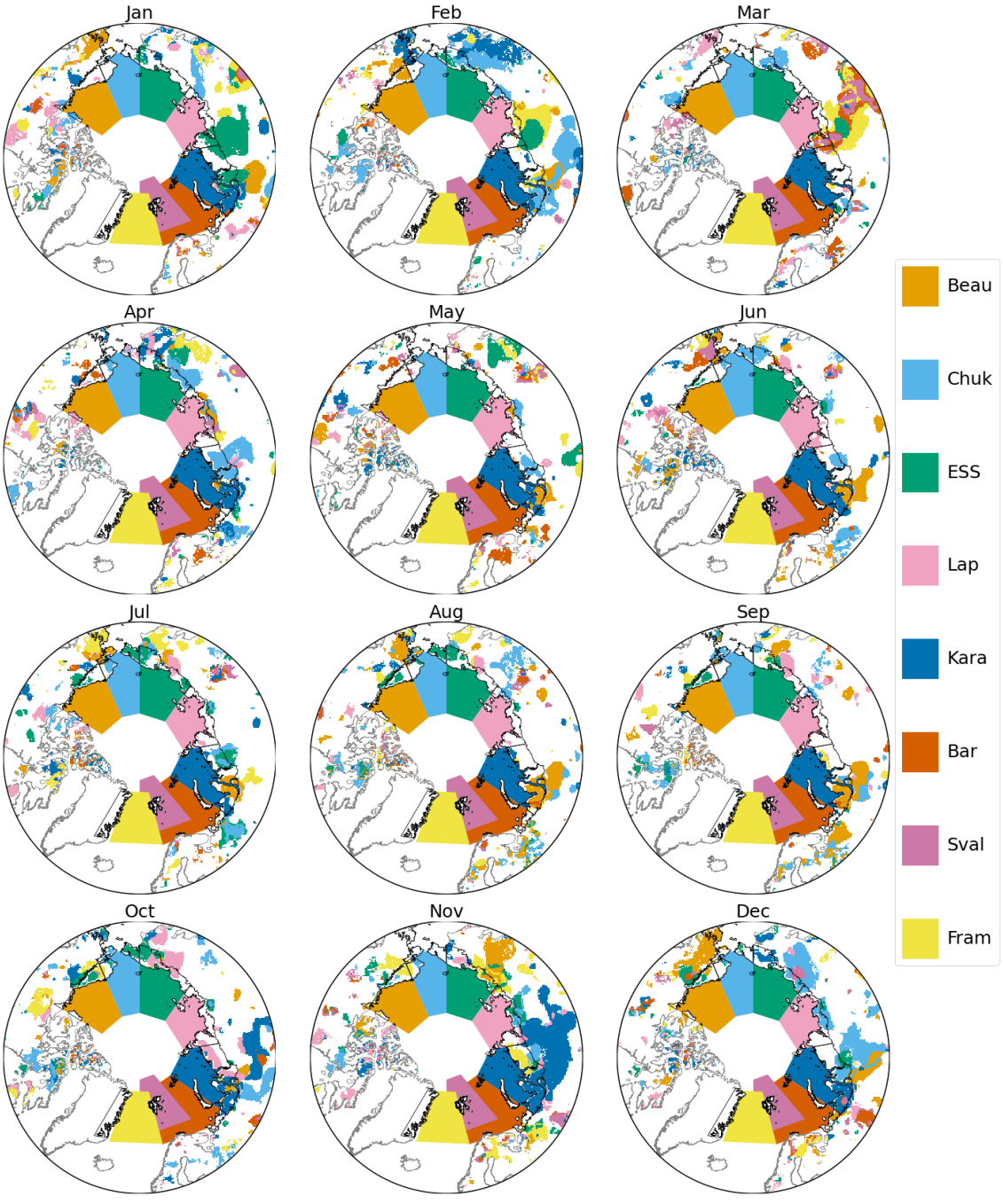


**Figure A14.** Area with significant maximum correlation of SWE (March) with sea ice area and associated basin (OSI SAF and EUMETSAT SAF On Ocean And Sea Ice, 2020), 2000-2019. For actual basin extent and legend see Figure 1.

https://doi.org/10.5194/egusphere-2025-1358
Preprint. Discussion started: 7 May 2025


*Author contributions.* AB developed the concept for the study, compiled the results and wrote the first draft of the manuscript. RT, HB, KR, JL, CvB and HT have processed the satellite data. MMF, HT, JL, BCF and CG contributed to the writing of the manuscript.

*Competing interests.* The authors declare no competing interests.

*Acknowledgements.* This work was supported by the CHARTER project and has received funding under the European Union's Horizon 2020 Research and Innovation Programme under Grant Agreement No 869471. This work was further supported by the European Space Agency CCI+ Permafrost (4000123681/18/I-NB), CCI+ Snow (4000124098/18/I-NB), and the European Research Council synergy Q-Arctic (No 951288) projects.

https://doi.org/10.5194/egusphere-2025-1358
Preprint. Discussion started: 7 May 2025


## References

Alexeev, V. A., Arp, C. D., Jones, B. M., and Cai, L.: Arctic sea ice decline contributes to thinning lake ice trend in northern Alaska, Environmental Research Letters, 11, 074 022, https://doi.org/10.1088/1748-9326/11/7/074022, 2016.

AMAP: Snow, Water, Ice and Permafrost in the Arctic (SWIPA) 2017. Arctic Monitoring and Assessment Programme (AMAP), Oslo, Norway. xiv + 269 pp, Tech. rep., Arctic Monitoring and Assessment Programme (AMAP), Oslo, 2017.

AMAP: AMAP Arctic Climate Change Update 2021: Key Trends and Impacts. Arctic Monitoring and Assessment Programme (AMAP), Tromsø, Norway. viii+148pp, Tech. rep., Arctic Monitoring and Assessment Programme (AMAP), Tromsø, 2021.

Anttila, K., Manninen, T., Jääskeläinen, E., Riihelä, A., and Lahtinen, P.: The Role of Climate and Land Use in the Changes in Surface Albedo Prior to Snow Melt and the Timing of Melt Season of Seasonal Snow in Northern Land Areas of 40°N–80°N during 1982–2015, Remote Sensing, 10, 1619, https://doi.org/10.3390/rs10101619, 2018.

Armstrong McKay, D. I., Staal, A., Abrams, J. F., Winkelmann, R., Sakschewski, B., Loriani, S., Fetzer, I., Cornell, S. E., Rockström, J., and Lenton, T. M.: Exceeding 1.5°C global warming could trigger multiple climate tipping points, Science, 377, https://doi.org/10.1126/science.abn7950, 2022.

Bartsch, A., Bergstedt, H., Pointner, G., Muri, X., Rautiainen, K., Leppänen, L., Joly, K., Sokolov, A., Orekhov, P., Ehrich, D., and Soininen, E. M.: Towards long-term records of rain-on-snow events across the Arctic from satellite data, The Cryosphere, 17, 889–915, https://doi.org/10.5194/tc-17-889-2023, 2023a.

Bartsch, A., Strozzi, T., and Nitze, I.: Permafrost Monitoring from Space, Surveys in Geophysics, https://doi.org/10.1007/s10712-023-09770-3, 2023b.

Bartsch, A., Tanguy, R., Bergstedt, H., Muri, X., and von Baeckmann, C.: Similarities in Northern Hemisphere Permafrost Ground Temperature and Sea Ice Extent Change from 1997 to 2019, in: IGARSS 2024 - 2024 IEEE International Geoscience and Remote Sensing Symposium, pp. 134–137, IEEE, https://doi.org/10.1109/igarss53475.2024.10642186, 2024.

Bartsch, A., Bergstedt, H., Tømmervik, H., Lemmetyinen, J., and Rautiainen, K.: Selected Arctic Land Parameter Trends: Ground Temperature, Snow Water Equivalent, NDVI, LAI and Freeze Thaw Duration, https://doi.org/10.5281/ZENODO.14975145, 2025a.

Bartsch, A., Muri, X., Hetzenecker, M., Rautiainen, K., Bergstedt, H., Wuite, J., Nagler, T., and Nicolsky, D.: Benchmarking passive-microwave-satellite-derived freeze–thaw datasets, The Cryosphere, 19, 459–483, https://doi.org/10.5194/tc-19-459-2025, 2025b.

Bartsch, A., Tanguy, R., Tømmervik, H., Lemmetyinen, J., Bergstedt, H., and von Baeckmann, C.: Arctic Sea Ice and Land Parameter Correlations (ASILaC), https://doi.org/10.5281/ZENODO.14975004, 2025c.

Berner, L. T., Massey, R., Jantz, P., Forbes, B. C., Macias-Fauria, M., Myers-Smith, I., Kumpula, T., Gauthier, G., Andreu-Hayles, L., Gaglioti, B. V., Burns, P., Zetterberg, P., D'Arrigo, R., and Goetz, S. J.: Summer warming explains widespread but not uniform greening in the Arctic tundra biome, Nature Communications, 11, https://doi.org/10.1038/s41467-020-18479-5, 2020.

Bhatt, U., Walker, D., Raynolds, M., Bieniek, P., Epstein, H., Comiso, J., Pinzon, J., Tucker, C., and Polyakov, I.: Recent Declines in Warming and Vegetation Greening Trends over Pan-Arctic Tundra, Remote Sensing, 5, 4229–4254, https://doi.org/10.3390/rs5094229, 2013.

Bhatt, U. S., Walker, D. A., Raynolds, M. K., Comiso, J. C., Epstein, H. E., Jia, G., Gens, R., Pinzon, J. E., Tucker, C. J., Tweedie, C. E., and Webber, P. J.: Circumpolar Arctic Tundra Vegetation Change Is Linked to Sea Ice Decline, Earth Interactions, 14, 1–20, https://doi.org/10.1175/2010EI315.1, 2010.

https://doi.org/10.5194/egusphere-2025-1358
Preprint. Discussion started: 7 May 2025


Bhatt, U. S., Walker, D. A., Raynolds, M. K., Bieniek, P. A., Epstein, H. E., Comiso, J. C., Pinzon, J. E., Tucker, C. J., Steele, M., Ermold, W., and Zhang, J.: Changing seasonality of panarctic tundra vegetation in relationship to climatic variables, Environmental Research Letters, 12, 055 003, https://doi.org/10.1088/1748-9326/aa6b0b, 2017.

Bhatt, U. S., Walker, D. A., Raynolds, M. K., Walsh, J. E., Bieniek, P. A., Cai, L., Comiso, J. C., Epstein, H. E., Frost, G. V., Gersten, R., Hendricks, A. S., Pinzon, J. E., Stock, L., and Tucker, C. J.: Climate drivers of Arctic tundra variability and change using an indicators framework, Environmental Research Letters, 16, 055 019, https://doi.org/10.1088/1748-9326/abe676, 2021.

Bjerke, J. W., López-Blanco, E., Tømmervik, H., Striberny, A., Davids, C., Ólafsdóttir, R., Karlsen, S. R., Sandström, P., Turunen, M., Rikkonen, T., Arneberg, M. K., Siikavuopio, S., Zinglersen, K., Lynge-Pedersen, K., Sandström, S., and Rautio, P.: Nordic boreo-arctic lands under rapid climatic change: A review of recent and future trends and extreme events, Earth-Science Reviews, 261, 105 012, https://doi.org/10.1016/j.earscirev.2024.105012, 2025.

Bokhorst, S. F., Bjerke, J. W., Tømmervik, H., Callaghan, T. V., and Phoenix, G. K.: Winter warming events damage sub-Arctic vegetation: consistent evidence from an experimental manipulation and a natural event, Journal of Ecology, 97, 1408–1415, https://doi.org/10.1111/j.1365-2745.2009.01554.x, 2009.

Brouillette, M.: How microbes in permafrost could trigger a massive carbon bomb, Nature, 591, 360–362, https://doi.org/10.1038/d41586-021-00659-y, 2021.

Buchwal, A., Sullivan, P. F., Macias-Fauria, M., Post, E., Myers-Smith, I. H., Stroeve, J. C., Blok, D., Tape, K. D., Forbes, B. C., Ropars, P., Lévesque, E., Elberling, B., Angers-Blondin, S., Boyle, J. S., Boudreau, S., Boulanger-Lapointe, N., Gamm, C., Hallinger, M., Rachlewicz, G., Young, A., Zetterberg, P., and Welker, J. M.: Divergence of Arctic shrub growth associated with sea ice decline, Proceedings of the National Academy of Sciences, 117, 33 334–33 344, https://doi.org/10.1073/pnas.2013311117, 2020.

Comiso, J. C. and Hall, D. K.: Climate trends in the Arctic as observed from space, WIREs Climate Change, 5, 389–409, https://doi.org/10.1002/wcc.277, 2014.

Comiso, J. C. and Nishio, F.: Trends in the sea ice cover using enhanced and compatible AMSR-E, SSM/I, and SMMR data, Journal of Geophysical Research: Oceans, 113, https://doi.org/10.1029/2007jc004257, 2008.

Druckenmiller, M. L., Moon, T. A., Thoman, R. L., Ballinger, T. J., Berner, L. T., Bernhard, G. H., Bhatt, U. S., Bjerke, J. W., Box, J. E., Brown, R., Cappelen, J., Christiansen, H. H., Decharme, B., Derksen, C., Divine, D., Drozdov, D. S., Elias Chereque, A., Epstein, H. E., Farquharson, L. M., Farrell, S. L., Fausto, R. S., Fettweis, X., Fioletov, V. E., Forbes, B. C., Frost, G. V., Gargulinski, E., Gerland, S., Goetz, S. J., Grabinski, Z., Grooß, J.-U., Haas, C., Hanna, E., Hanssen-Bauer, I., Hendricks, S., Holmes, R. M., Ialongo, I., Isaksen, K., Jain, P., Johnsen, B., Kaleschke, L., Kholodov, A. L., Kim, S.-J., Korsgaard, N. J., Labe, Z., Lakkala, K., Lara, M. J., Loomis, B., Luojus, K., Macander, M. J., Malkova, G. V., Mankoff, K. D., Manney, G. L., McClelland, J. W., Meier, W. N., Mote, T., Mudryk, L., Müller, R., Nyland, K. E., Overland, J. E., Park, T., Pavlova, O., Perovich, D., Petty, A., Phoenix, G. K., Raynolds, M. K., Reijmer, C. H., Richter-Menge, J., Ricker, R., Romanovsky, V. E., Scott, L., Shapiro, H., Shiklomanov, A. I., Shiklomanov, N. I., Smeets, C. J. P. P., Smith, S. L., Soja, A., Spencer, R. G. M., Starkweather, S., Streletskiy, D. A., Suslova, A., Svendby, T., Tank, S. E., Tedesco, M., Tian-Kunze, X., Timmermans, M.-L., Tømmervik, H., Tretiakov, M., Tschudi, M., Vakhutinsky, S., van As, D., van de Wal, R. S. W., Veraverbeke, S., Walker, D. A., Walsh, J. E., Wang, M., Webster, M., Winton, O., Wood, K., York, A., and Ziel, R.: The Arctic, Bulletin of the American Meteorological Society, 102, S263–S316, https://doi.org/10.1175/bams-d-21-0086.1, 2021.

Dupuis, S., Göttsche, F.-M., and Wunderle, S.: Temporal stability of a new 40-year daily AVHRR land surface temperature dataset for the pan-Arctic region, The Cryosphere, 18, 6027–6059, https://doi.org/10.5194/tc-18-6027-2024, 2024.

https://doi.org/10.5194/egusphere-2025-1358
Preprint. Discussion started: 7 May 2025


Dutrieux, L. P., Bartholomeus, H., Herold, M., and Verbesselt, J.: Relationships between declining summer sea ice, increasing temperatures and changing vegetation in the Siberian Arctic tundra from MODIS time series (2000–11), Environmental Research Letters, 7, 044 028, https://doi.org/10.1088/1748-9326/7/4/044028, 2012.

Forbes, B. C., Kumpula, T., Meschtyb, N., Laptander, R., Macias-Fauria, M., Zetterberg, P., Verdonen, M., Skarin, A., Kim, K.-Y., Boisvert, L. N., Stroeve, J. C., and Bartsch, A.: Sea ice, rain-on-snow and tundra reindeer nomadism in Arctic Russia, Biology Letters, https://doi.org/10.1098/rsbl.2016.0466, 2016.

Frost, e.: The changing face of the Arctic: four decades of greening and implications for tundra ecosystems., Front. Environ. Sci, 13, 1525 574., https://doi.org/10.3389/fenvs.2025.1525574, 2025.

Gastineau, G., Frankignoul, C., Gao, Y., Liang, Y.-C., Kwon, Y.-O., Cherchi, A., Ghosh, R., Manzini, E., Matei, D., Mecking, J., Suo, L., Tian, T., Yang, S., and Zhang, Y.: Forcing and impact of the Northern Hemisphere continental snow cover in 1979–2014, The Cryosphere, 17, 2157–2184, https://doi.org/10.5194/tc-17-2157-2023, 2023.

Heim, B., Lisovski, S., Wieczorek, M., Pellet, C., Delaloye, R., Bartsch, A., Jakober, D., Pointner, G., and Strozzi, T.: ESA CCI+ Product Validation and Intercomparison Report, v3.0, Tech. rep., 2021.

IPCC: IPCC Special Report on the Ocean and Cryosphere in a Changing Climate, 2019.

Karlsen, S. R., Elvebakk, A., Stendardi, L., Høgda, K. A., and Macias-Fauria, M.: Greening of Svalbard, Science of The Total Environment, 945, 174 130, https://doi.org/10.1016/j.scitotenv.2024.174130, 2024.

Kerby, J. T. and Post, E.: Advancing plant phenology and reduced herbivore production in a terrestrial system associated with sea ice decline, Nature Communications, 4, https://doi.org/10.1038/ncomms3514, 2013.

Kim, Y., Kimball, J. S., Glassy, J., and Du, J.: An extended global Earth system data record on daily landscape freeze–thaw status determined from satellite passive microwave remote sensing, Earth System Science Data, 9, 133–147, https://doi.org/10.5194/essd-9-133-2017, 2017.

Kim, Y., Kimball, J., Du, J., and Glassy, J.: MEaSUREs Global Record of Daily Landscape Freeze/Thaw Status, Version 5, https://doi.org/10.5067/LJ6SLXNJB2CQ, 2021.

Lenton, T. M., Held, H., Kriegler, E., Hall, J. W., Lucht, W., Rahmstorf, S., and Schellnhuber, H. J.: Tipping elements in the Earth's climate system, Proceedings of the National Academy of Sciences, 105, 1786–1793, https://doi.org/10.1073/pnas.0705414105, 2008.

Lenton, T. M., Abrams, J. F., Bartsch, A., Bathiany, S., Boulton, C. A., Buxton, J. E., Conversi, A., Cunliffe, A. M., Hebden, S., Lavergne, T., Poulter, B., Shepherd, A., Smith, T., Swingedouw, D., Winkelmann, R., and Boers, N.: Remotely sensing potential climate change tipping points across scales, Nature Communications, 15, https://doi.org/10.1038/s41467-023-44609-w, 2024.

Letterly, A., Key, J., and Liu, Y.: Arctic climate: changes in sea ice extent outweigh changes in snow cover, The Cryosphere, 12, 3373–3382, https://doi.org/10.5194/tc-12-3373-2018, 2018.

Li, M., Cao, S., Zhu, Z., Wang, Z., Myneni, R. B., and Piao, S.: Spatiotemporally consistent global dataset of the GIMMS Normalized Difference Vegetation Index (PKU GIMMS NDVI) from 1982 to 2022, Earth System Science Data, 15, 4181–4203, https://doi.org/10.5194/essd-15-4181-2023, 2023.

Liu, C., Huang, H., Liu, C., Wang, X., and Wang, S.: Comparative evaluation of vegetation greenness trends over circumpolar Arctic tundra using multi-sensors satellite datasets, International Journal of Digital Earth, 17, https://doi.org/10.1080/17538947.2024.2328823, 2024.

Luojus, K., Pulliainen, J., Takala, M., Lemmetyinen, J., Mortimer, C., Derksen, C., Mudryk, L., Moisander, M., Hiltunen, M., Smolander, T., Ikonen, J., Cohen, J., Salminen, M., Norberg, J., Veijola, K., and Venäläinen, P.: GlobSnow v3.0 Northern Hemisphere snow water equivalent dataset, Scientific Data, 8, https://doi.org/10.1038/s41597-021-00939-2, 2021.

https://doi.org/10.5194/egusphere-2025-1358
Preprint. Discussion started: 7 May 2025


Macias-Fauria, M., Forbes, B. C., Zetterberg, P., and Kumpula, T.: Eurasian Arctic greening reveals teleconnections and the potential for structurally novel ecosystems, Nature Climate Change, 2, 613–618, https://doi.org/10.1038/nclimate1558, 2012.

Macias-Fauria, M., Karlsen, S. R., and Forbes, B. C.: Disentangling the coupling between sea ice and tundra productivity in Svalbard, Scientific Reports, 7, https://doi.org/10.1038/s41598-017-06218-8, 2017.

Mekonnen, Z. A., Riley, W. J., Berner, L. T., Bouskill, N. J., Torn, M. S., Iwahana, G., Breen, A. L., Myers-Smith, I. H., Criado, M. G., Liu, Y., Euskirchen, E. S., Goetz, S. J., Mack, M. C., and Grant, R. F.: Arctic tundra shrubification: a review of mechanisms and impacts on ecosystem carbon balance, Environmental Research Letters, 16, 053 001, https://doi.org/10.1088/1748-9326/abf28b, 2021.

Miner, K. R., Turetsky, M. R., Malina, E., Bartsch, A., Tamminen, J., McGuire, A. D., Fix, A., Sweeney, C., Elder, C. D., and Miller, C. E.: Permafrost carbon emissions in a changing Arctic, Nature Reviews Earth & Environment, 3, 55–67, https://doi.org/10.1038/s43017-021-00230-3, 2022.

Myers-Smith, I. H., Kerby, J. T., Phoenix, G. K., Bjerke, J. W., Epstein, H. E., Assmann, J. J., John, C., Andreu-Hayles, L., Angers-Blondin, S., Beck, P. S. A., Berner, L. T., Bhatt, U. S., Bjorkman, A. D., Blok, D., Bryn, A., Christiansen, C. T., Cornelissen, J. H. C., Cunliffe, A. M., Elmendorf, S. C., Forbes, B. C., Goetz, S. J., Hollister, R. D., de Jong, R., Loranty, M. M., Macias-Fauria, M., Maseyk, K., Normand, S., Olofsson, J., Parker, T. C., Parmentier, F.-J. W., Post, E., Schaepman-Strub, G., Stordal, F., Sullivan, P. F., Thomas, H. J. D., Tømmervik, H., Treharne, R., Tweedie, C. E., Walker, D. A., Wilmking, M., and Wipf, S.: Complexity revealed in the greening of the Arctic, Nature Climate Change, 10, 106–117, https://doi.org/10.1038/s41558-019-0688-1, 2020.

Obu, J., Westermann, S., Bartsch, A., Berdnikov, N., Christiansen, H. H., Dashtseren, A., Delaloye, R., Elberling, B., Etzelmüller, B., Kholodov, A., Khomutov, A., Kääb, A., Leibman, M. O., Lewkowicz, A. G., Panda, S. K., Romanovsky, V., Way, R. G., Westergaard-Nielsen, A., Wu, T., Yamkhin, J., and Zou, D.: Northern Hemisphere permafrost map based on TTOP modelling for 2000-2016 at 1?km2 scale, Earth-Science Reviews, 193, 299–316, https://doi.org/10.1016/j.earscirev.2019.04.023, 2019.

Obu, J., Westermann, S., Barboux, C., Bartsch, A., Delaloye, R., Grosse, G., Heim, B., Hugelius, G., Irrgang, A., Kääb, A. M., Kroisleitner, C., Matthes, H., Nitze, I., Pellet, C., Seifert, F. M., Strozzi, T., Wegmüller, U., Wieczorek, M., and Wiesmann, A.: ESA Permafrost Climate Change Initiative (Permafrost_cci): Permafrost ground temperature for the Northern Hemisphere, v3.0, CEDA, https://doi.org/10.5285/b25d4a6174de4ac78000d034f500a268, 2021a.

Obu, J., Westermann, S., Barboux, C., Bartsch, A., Delaloye, R., Grosse, G., Heim, B., Hugelius, G., Irrgang, A., Kääb, A. M., Kroisleitner, C., Matthes, H., Nitze, I., Pellet, C., Seifert, F. M., Strozzi, T., Wegmüller, U., Wieczorek, M., and Wiesmann, A.: ESA Permafrost Climate Change Initiative (Permafrost_cci): Permafrost extent for the Northern Hemisphere, v3.0, CEDA, https://doi.org/10.5285/6e2091cb0c8b4106921b63cd5357c97c, 2021b.

OSI SAF and EUMETSAT SAF On Ocean And Sea Ice: Sea Ice Index - Multimission, https://doi.org/10.15770/EUM_SAF_OSI_0022, data extracted from OSI SAF FTP server: 2000-2019, accessed 2023, 2020.

Park, H., Walsh, J. E., Kim, Y., Nakai, T., and Ohata, T.: The role of declining Arctic sea ice in recent decreasing terrestrial Arctic snow depths, Polar Science, 7, 174–187, https://doi.org/10.1016/j.polar.2012.10.002, 2013.

Park, T., Ganguly, S., Tømmervik, H., Euskirchen, E. S., Høgda, K.-A., Karlsen, S. R., Brovkin, V., Nemani, R. R., and Myneni, R. B.: Changes in growing season duration and productivity of northern vegetation inferred from long-term remote sensing data, Environmental Research Letters, 11, 084 001, https://doi.org/10.1088/1748-9326/11/8/084001, 2016.

Pedersen, A., Soininen, E., Hansen, B., Le Moullec, M., Loe, L., Paulsen, I., Eischeid, I., Karlsen, S., Ropstad, E., Stien, A., Tarroux, A., Tommervik, H., and Ravolainen, V.: High seasonal overlap in habitat suitability in a non-migratory High Arctic ungulate, Global Ecology and Conservation, 45, e02 528, https://doi.org/10.1016/j.gecco.2023.e02528, 2023.

https://doi.org/10.5194/egusphere-2025-1358
Preprint. Discussion started: 7 May 2025


Peeters, B., Le Moullec, M., Raeymaekers, J. A. M., Marquez, J. F., Røed, K. H., Pedersen, A. O., Veiberg, V., Loe, L. E., and Hansen, B. B.: Sea ice loss increases genetic isolation in a high Arctic ungulate metapopulation, Global Change Biology, 26, 2028–2041, https://doi.org/10.1111/gcb.14965, 2020.

Pinzon, J. and Tucker, C.: A Non-Stationary 1981–2012 AVHRR NDVI3g Time Series, Remote Sensing, 6, 6929–6960, https://doi.org/10.3390/rs6086929, 2014.

Pulliainen, J., Luojus, K., Derksen, C., Mudryk, L., Lemmetyinen, J., Salminen, M., Ikonen, J., Takala, M., Cohen, J., Smolander, T., and Norberg, J.: Patterns and trends of Northern Hemisphere snow mass from 1980 to 2018, Nature, 581, 294–298, https://doi.org/10.1038/s41586-020-2258-0, 2020.

Rantanen, M., Karpechko, A. Y., Lipponen, A., Nordling, K., Hyvärinen, O., Ruosteenoja, K., Vihma, T., and Laaksonen, A.: The Arctic has warmed nearly four times faster than the globe since 1979, Communications Earth & Environment, 3, https://doi.org/10.1038/s43247-022-00498-3, 2022.

Raynolds, M. K., Walker, D. A., Balser, A., Bay, C., Campbell, M., Cherosov, M. M., Daniëls, F. J., Eidesen, P. B., Ermokhina, K. A., Frost, G. V., Jedrzejek, B., Jorgenson, M. T., Kennedy, B. E., Kholod, S. S., Lavrinenko, I. A., Lavrinenko, O. V., Magnússon, B., Matveyeva, N. V., Metúsalemsson, S., Nilsen, L., Olthof, I., Pospelov, I. N., Pospelova, E. B., Pouliot, D., Razzhivin, V., Schaepman-Strub, G., Šibík, J., Telyatnikov, M. Y., and Troeva, E.: A raster version of the Circumpolar Arctic Vegetation Map (CAVM), Remote Sensing of Environment, 232, 111 297, https://doi.org/10.1016/j.rse.2019.111297, 2019.

Rixen, C., Høye, T. T., Macek, P., Aerts, R., Alatalo, J. M., Anderson, J. T., Arnold, P. A., Barrio, I. C., Bjerke, J. W., Björkman, M. P., Blok, D., Blume-Werry, G., Boike, J., Bokhorst, S., Carbognani, M., Christiansen, C. T., Convey, P., Cooper, E. J., Cornelissen, J. H. C., Coulson, S. J., Dorrepaal, E., Elberling, B., Elmendorf, S. C., Elphinstone, C., Forte, T. G., Frei, E. R., Geange, S. R., Gehrmann, F., Gibson, C., Grogan, P., Halbritter, A. H., Harte, J., Henry, G. H., Inouye, D. W., Irwin, R. E., Jespersen, G., Jónsdóttir, I. S., Jung, J. Y., Klinges, D. H., Kudo, G., Lämsä, J., Lee, H., Lembrechts, J. J., Lett, S., Lynn, J. S., Mann, H. M., Mastepanov, M., Morse, J., Myers-Smith, I. H., Olofsson, J., Paavola, R., Petraglia, A., Phoenix, G. K., Semenchuk, P., Siewert, M. B., Slatyer, R., Spasojevic, M. J., Suding, K., Sullivan, P., Thompson, K. L., Väisänen, M., Vandvik, V., Venn, S., Walz, J., Way, R., Welker, J. M., Wipf, S., and Zong, S.: Winters are changing: snow effects on Arctic and alpine tundra ecosystems, Arctic Science, 8, 572–608, https://doi.org/10.1139/as-2020-0058, 2022.

Sasgen, I., Steinhoefel, G., Kasprzyk, C., Matthes, H., Westermann, S., Boike, J., and Grosse, G.: Atmosphere circulation patterns synchronize pan-Arctic glacier melt and permafrost thaw, Communications Earth & Environment, 5, 375, https://doi.org/10.1038/s43247-024-01548-8, 2024.

Smith, N. V., Saatchi, S. S., and Randerson, J. T.: Trends in high northern latitude soil freeze and thaw cycles from 1988 to 2002, Journal of Geophysical Research: Atmospheres, 109, https://doi.org/10.1029/2003JD004472, 2004.

Spreen, G., Kaleschke, L., and Heygster, G.: Sea ice remote sensing using AMSR-E 89-GHz channels, Journal of Geophysical Research, 113, https://doi.org/10.1029/2005jc003384, 2008.

Stroeve, J. and Notz, D.: Changing state of Arctic sea ice across all seasons, Environmental Research Letters, 13, 103 001, https://doi.org/10.1088/1748-9326/aade56, 2018.

Takala, M., Pulliainen, J., Metsamaki, S., and Koskinen, J.: Detection of Snowmelt Using Spaceborne Microwave Radiometer Data in Eurasia From 1979 to 2007, IEEE Transactions on Geoscience and Remote Sensing, 47, 2996–3007, https://doi.org/10.1109/TGRS.2009.2018442, 2009.

Tømmervik, H.: GLOBAL MODIS NDVI/LAI and NOAA AVHRR GIMMS NDVI datasets, https://doi.org/10.5281/ZENODO.14644910, 2025.

https://doi.org/10.5194/egusphere-2025-1358
Preprint. Discussion started: 7 May 2025


Vermote, E. and NOAA CDR Program: NOAA Climate Data Record (CDR) of AVHRR Normalized Difference Vegetation Index (NDVI), Version 5, https://doi.org/10.7289/V5ZG6QH9, accessed 2021, 2019.

Vikhamar-Schuler, D., Isaksen, K., Haugen, J. E., Tømmervik, H., Luks, B., Schuler, T. V., and Bjerke, J. W.: Changes in Winter Warming Events in the Nordic Arctic Region, Journal of Climate, 29, 6223–6244, https://doi.org/10.1175/jcli-d-15-0763.1, 2016.

Walker, D., Gould, W., Maier, H., and Raynolds, M.: The Circumpolar Arctic Vegetation Map: AVHRR-derived base maps, environmental controls, and integrated mapping procedures, International Journal of Remote Sensing, 23, 4551ï¿½4570, 2002.

Watts, J. D., Potter, S., Rogers, B. M., Virkkala, A., Fiske, G., Arndt, K. A., Burrell, A., Butler, K., Gerlt, B., Grayson, J., Shestakova, T. A., Du, J., Kim, Y., Parmentier, F. W., and Natali, S. M.: Regional Hotspots of Change in Northern High Latitudes Informed by Observations From Space, Geophysical Research Letters, 52, https://doi.org/10.1029/2023GL108081, 2025.

Westermann, S., Peter, M., Langer, M., Schwamborn, G., Schirrmeister, L., EtzelmÃ¼ller, B., and Boike, J.: Transient modeling of the ground thermal conditions using satellite data in the Lena River delta, Siberia, The Cryosphere, 11, 1441–1463, https://doi.org/10.5194/tc-11-1441-2017, 2017.

Yu, L., Leng, G., and Python, A.: Varying response of vegetation to sea ice dynamics over the Arctic, Science of The Total Environment, 799, 149 378, https://doi.org/10.1016/j.scitotenv.2021.149378, 2021.